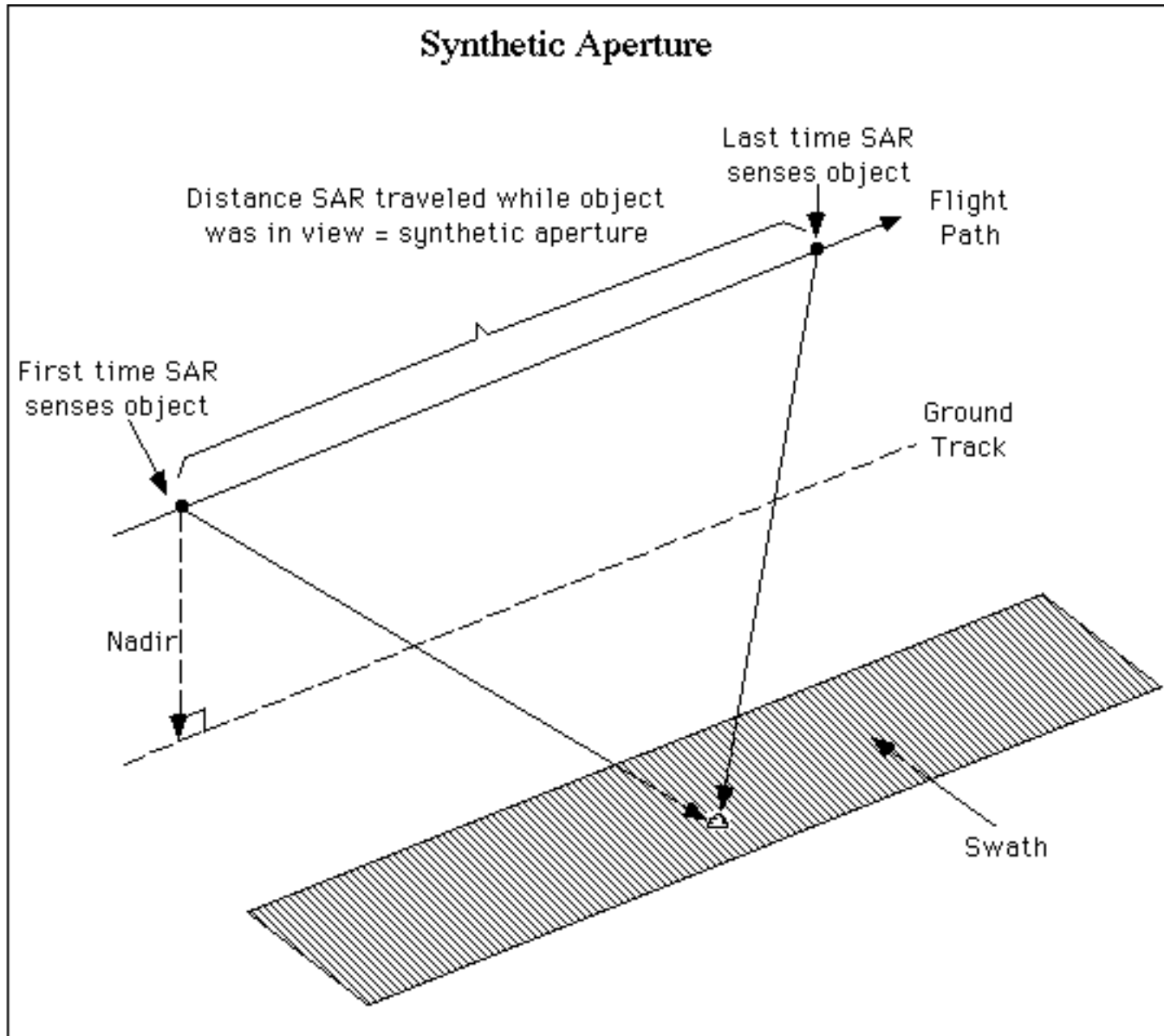


A target's backscatter will be analyzed as though it had been seen by 1000 different antennas, or correspondingly of a synthesized antenna with length equal to the distance the spacecraft passed through while it was able to get backscatter returns from that target



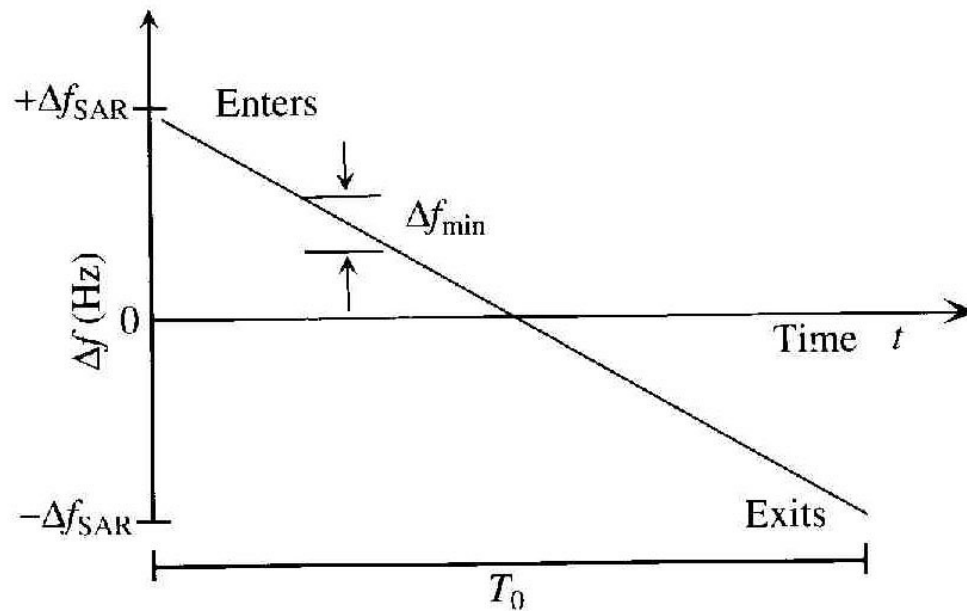
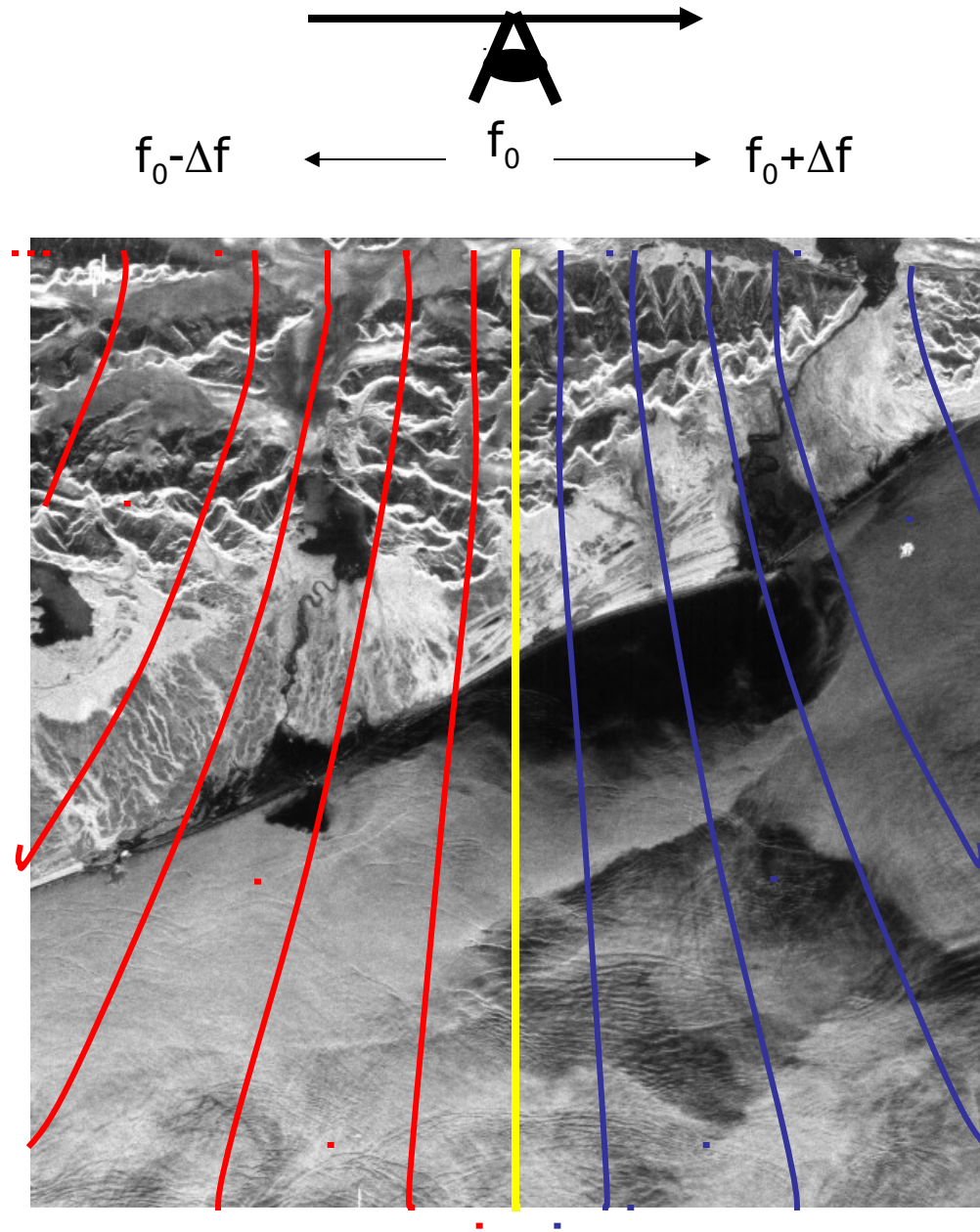


Figure 13.6. Tracking an object in frequency space across the SAR footprint, where the target enters at upper left and exits at lower right.

The SAR image is derived from the received power:

$$W(t, f)$$



# Radar Bands

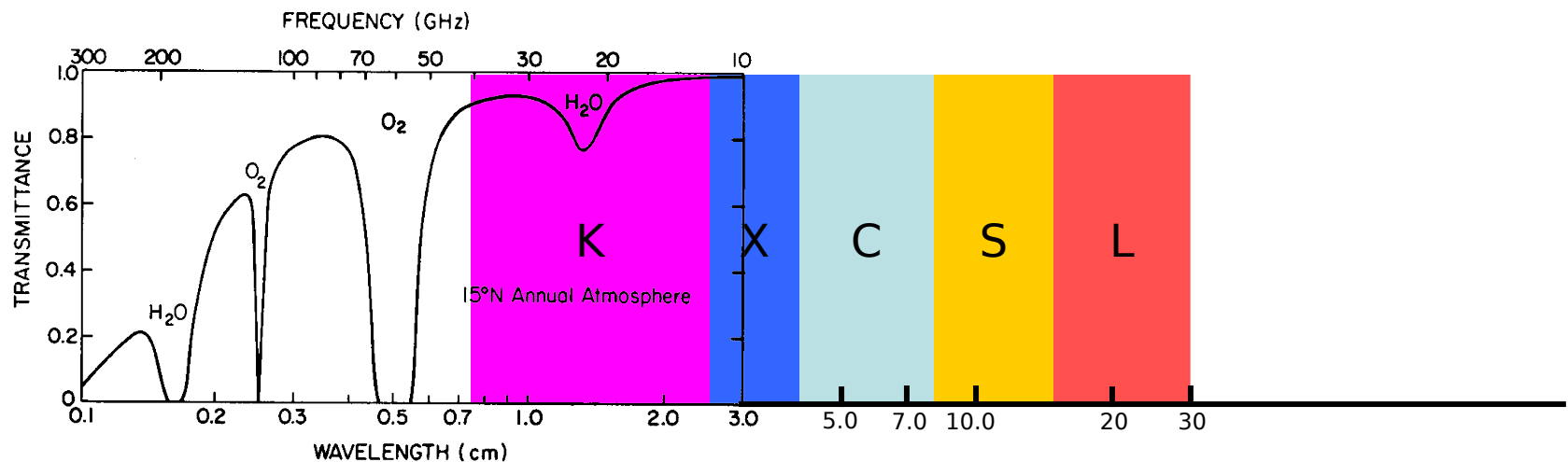
**L-Band:** 1-2 GHz, 15-30 cm wavelength (23 cm common).

**S-Band:** 2-4 GHz, 08-15 cm wavelength (10 cm).

**C-Band:** 4-8 GHz, 04-08 cm wavelength (5 cm).

**X-Band:** 8-12 GHz, 2.5-4 cm wavelength (3 cm).

**K-Band:** (u) 12-18, (a) 27-40 GHz, 1.7-2.5, .75-1.2 cm wavelength (mm).





Ahmed, *et al.*, 1990; Raney, 1998

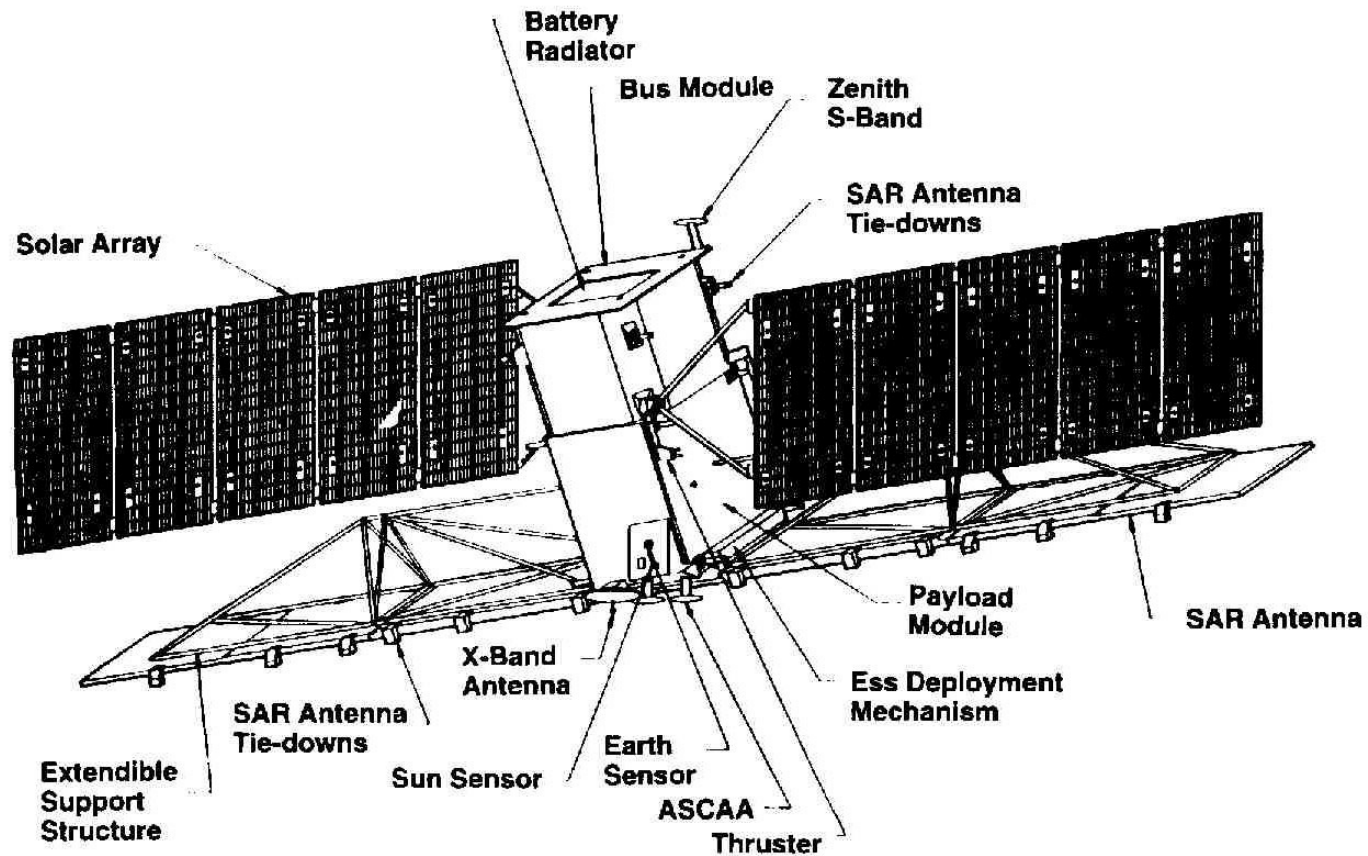


Figure 13.9. The configuration of the RADARSAT spacecraft; the antenna measures 15 m by 1.5 m. (Figure 1 from Moore *et al.* 1993, © 1993 Canadian Aeronautics and Space Institute, used with permission).

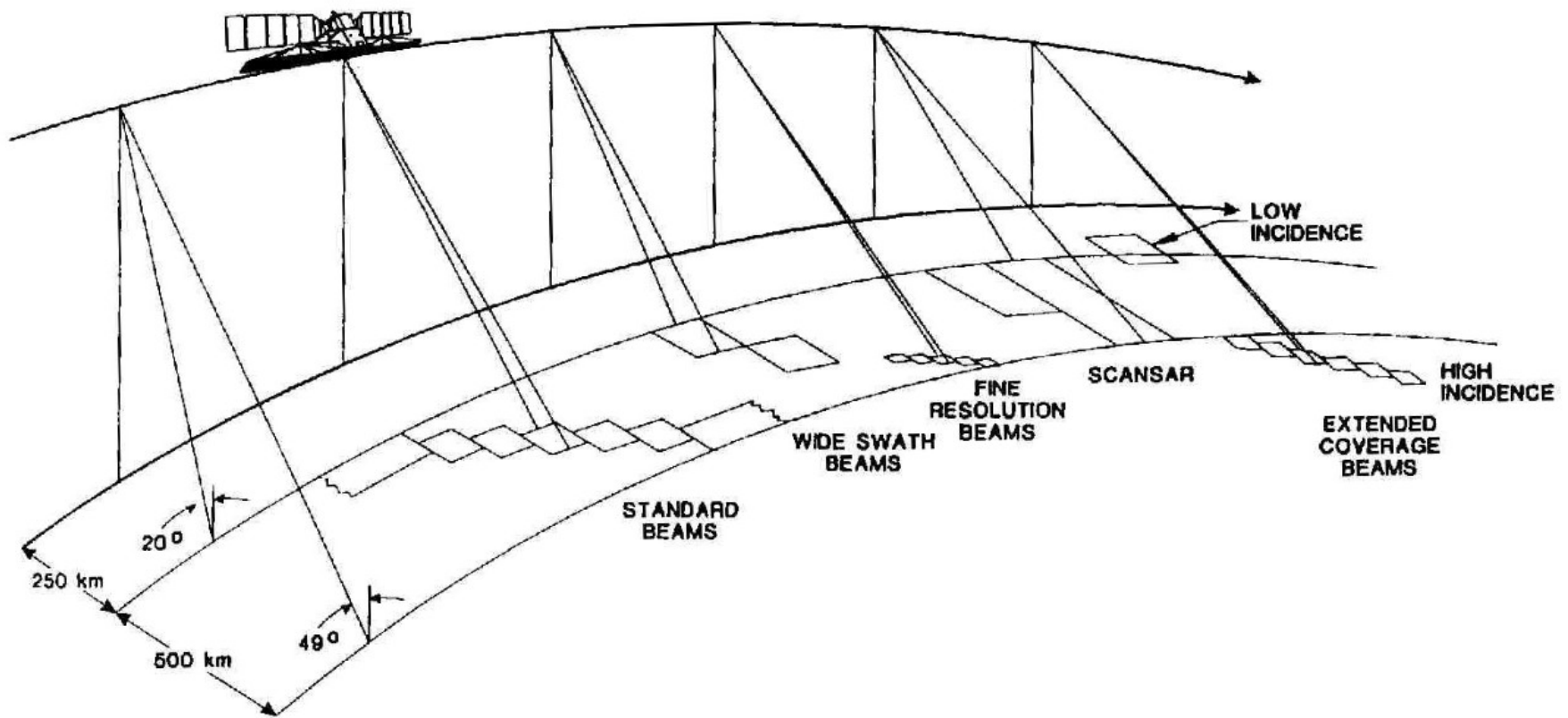
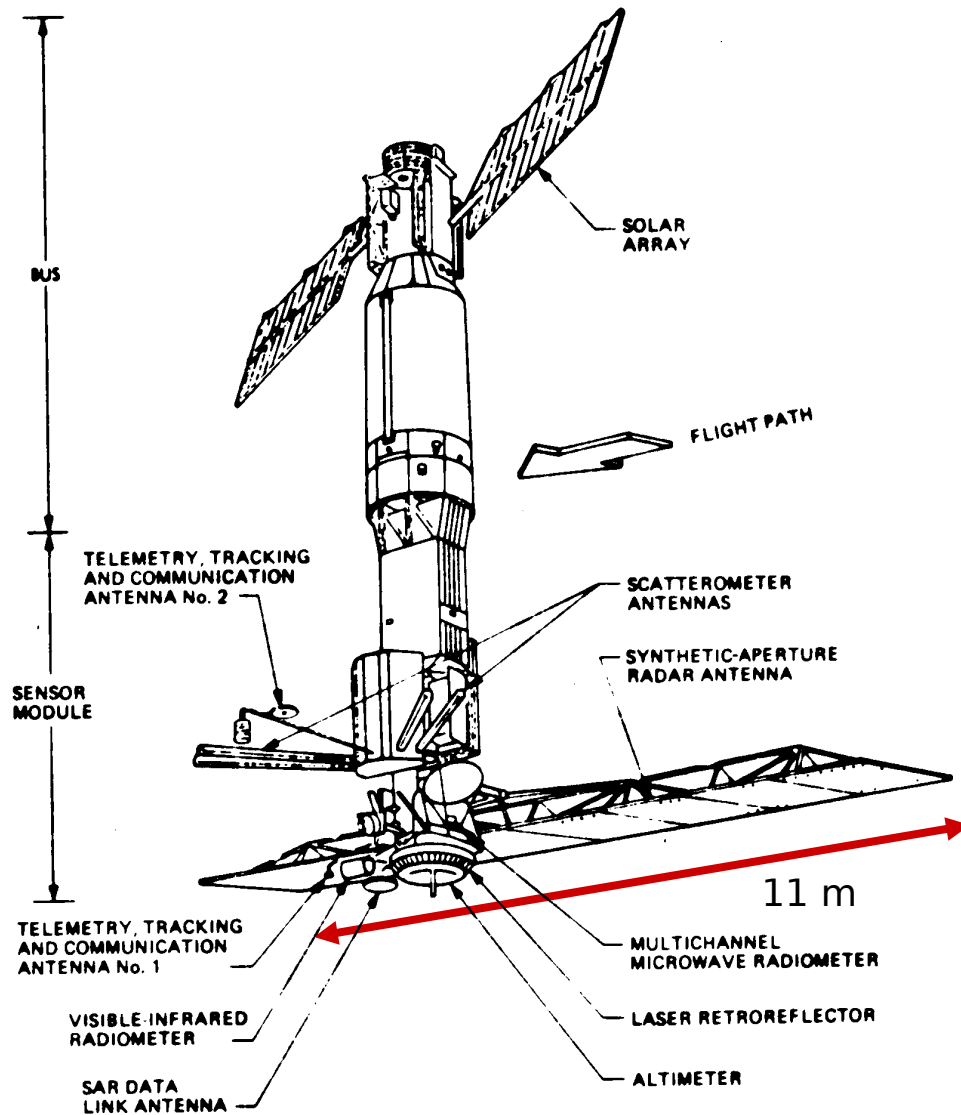
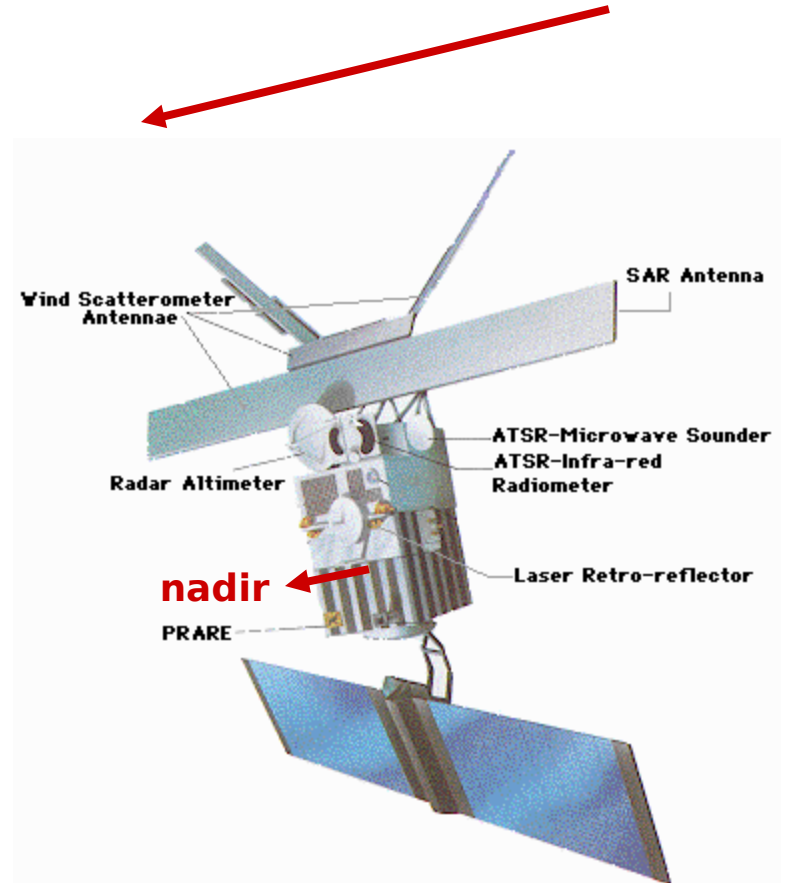


Figure 13.11. The different imaging modes for RADARSAT; see text and Table 13.3 for additional description (Figure 1 from Luscombe *et al.*, 1993, © 1993 Canadian Aeronautics and Space Institute, used with permission).

# SeaSat Satellite



## Satellite motion



## ERS Satellite

## Seasat SAR (*Synthetic Aperture Radar*)

L-band, HH polarization, fixed look angle

1275 MHz (23.5 cm) band

100 km swath width at 25 m resolution

Transmitted Pulse Length 33.4 microseconds

Antenna Dimensions 10.74 m x 2.16 m

Antenna Look Angle 20 degrees from vertical

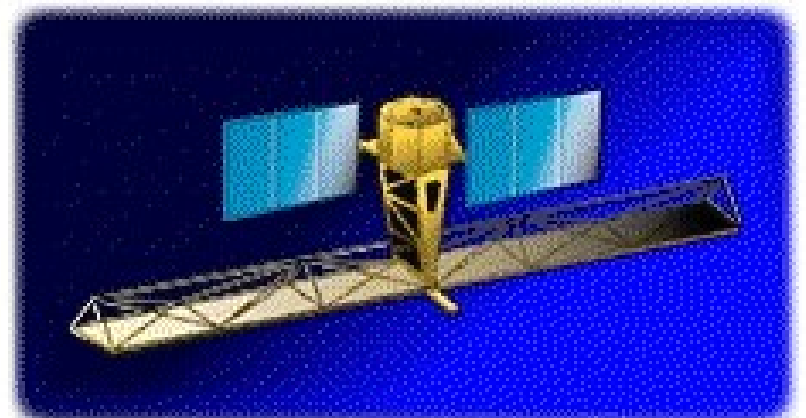
Pulse repetition frequency (PRF) 1463-1640 Hz

Incidence angle on the surface 23 degrees +/- 3 degrees across the swath

RADARSAT	5.3 GHz (C-Band)
ERS	5.3 GHz (C-Band)

The RADARSAT 2

Synthetic Aperture Radar (SAR) will acquire data at **horizontal (HH)**, **vertical (VV)** and **cross (HV)** polarizations over a range of resolutions from 100 to three metres.



# **SAR applications**

## ICE

ice edge  
ice motion  
ice thickness



Waves

Winds

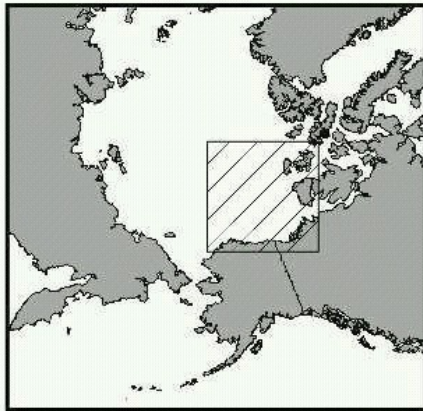
Currents


Ship Wakes

Slicks



# Beaufort Sea



 produced on the ASF's  
Interactive Image Analysis System (IIAS)

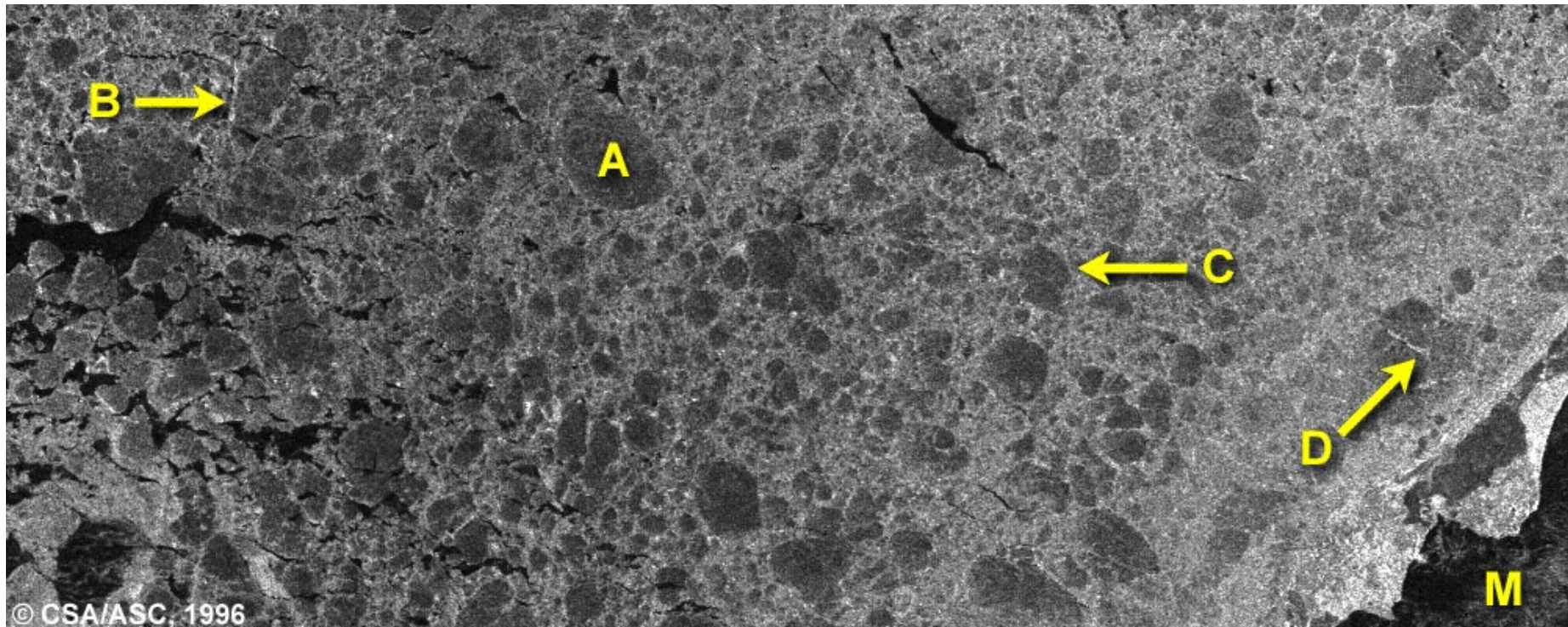
(c) ESA 1992





Ice Reconnaissance  
Gulf of St Lawrence, Eastern Canada  
March 6, 1996

Thin first year ice floes (**B**) and rough "brash ice" (**A**) are clearly visible as are pressure ridges (**C**) and cracks or "leads" within first year ice floes (**D**).





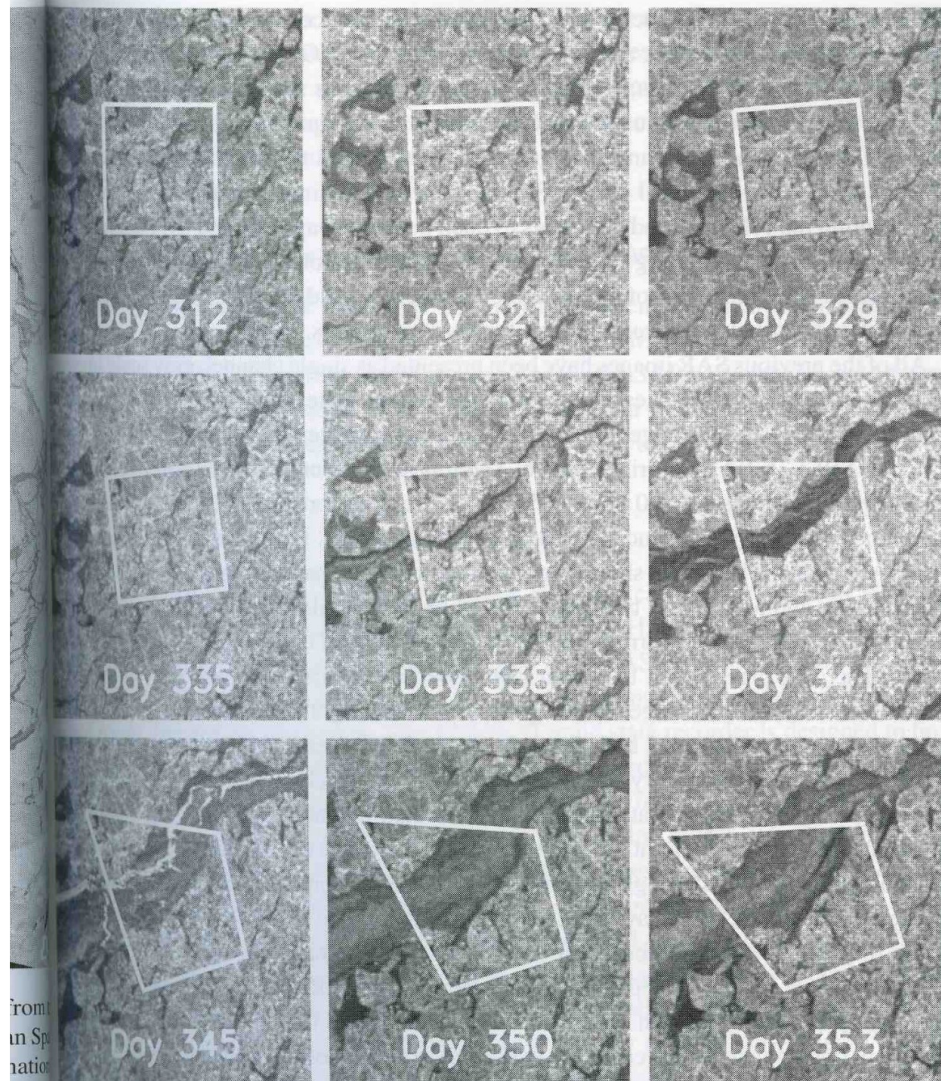
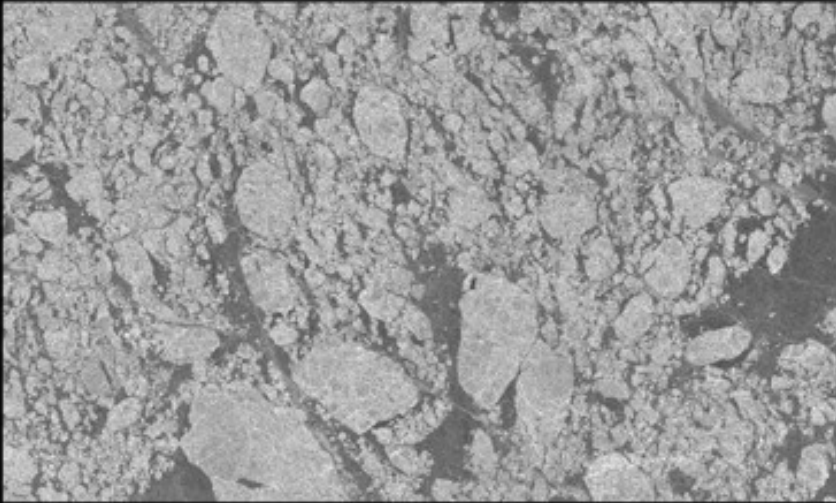
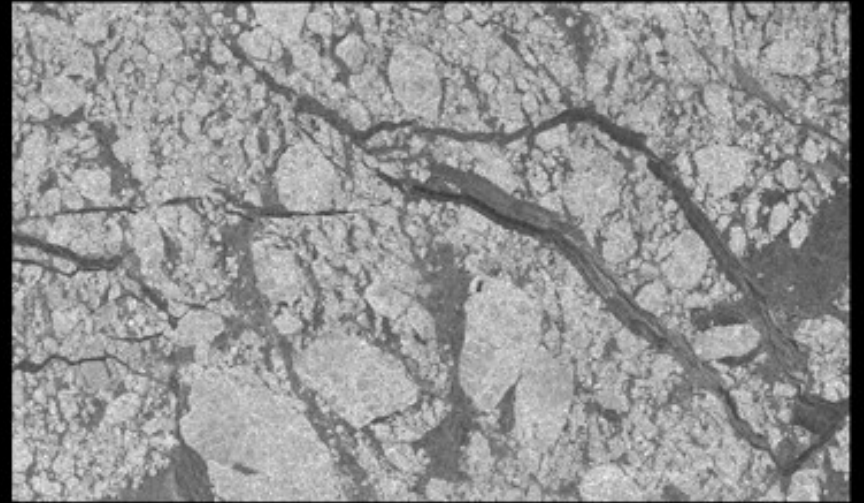


Figure 13.21. Time series of RADARSAT observations of sea ice at various intervals in the Beaufort Sea during 1996, showing the deformation of an initial 10-km square box over a 41-day period from Day 312 (November 8) to 353 (December 19). The white outlined square on Day 312 is the 10-km box; the successive images show its deformation (Figure 1 in Kwok *et al.* 1999, © 1999 American Geophysical Union, reproduced/modified by permission of AGU; RADARSAT data © Canadian Space Agency/Agence Spatiale Canadienne 1996. Processed and distributed by RADARSAT International, courtesy Ron Kwok).



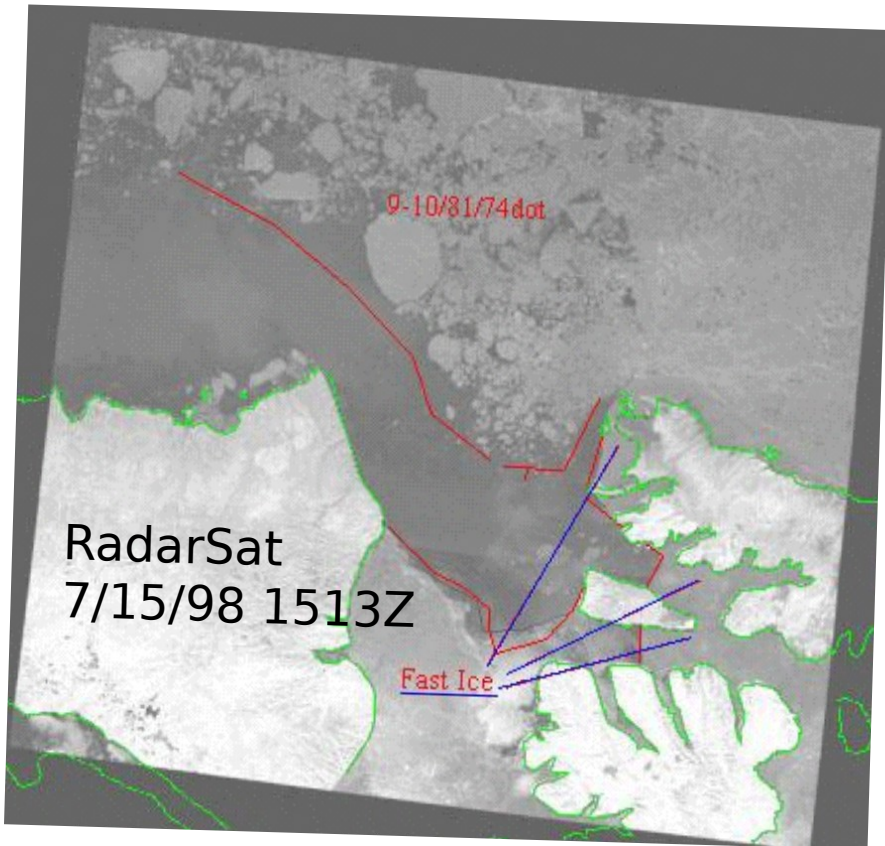


Day 1

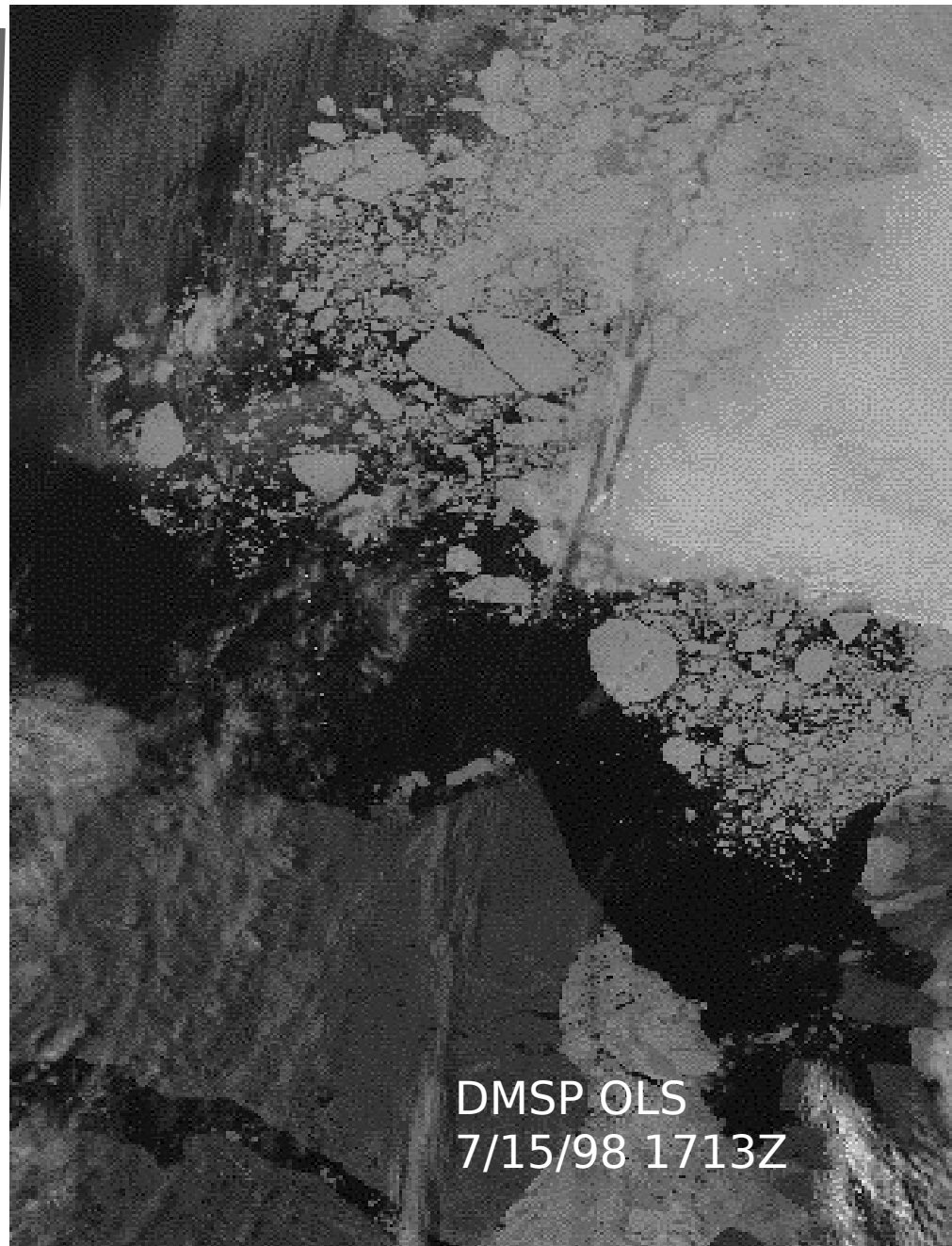


Day 9

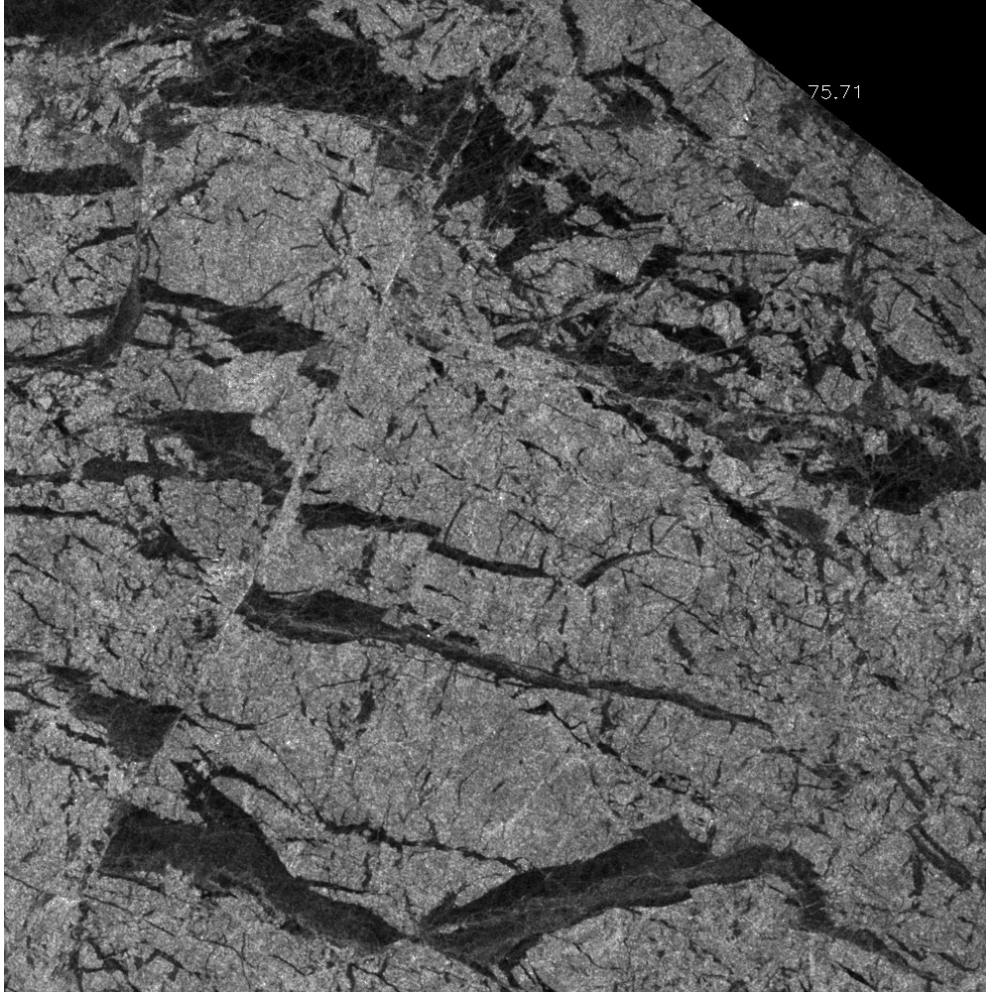
Radarsat data 96 x128km images

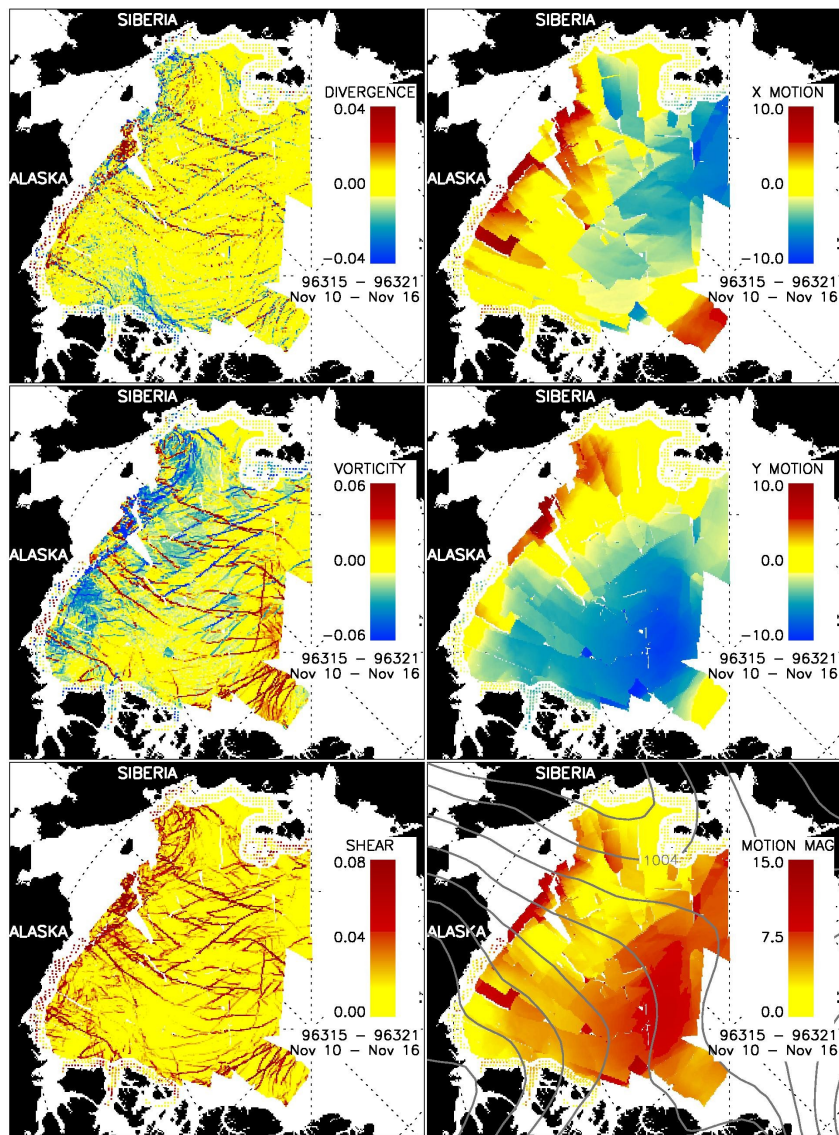


“All images are of the Beaufort Sea.  
The RadarSat image is focused on the  
northern part of Banks Island, in the  
northeastern Beaufort Sea.”



**\*\***[http://www-radar.jpl.nasa.gov/rgps/image\\_files/sheba1\\_a](http://www-radar.jpl.nasa.gov/rgps/image_files/sheba1_a)





# SAR applications

ICE

ice edge

ice motion

ice thicknesss

Waves



Winds

Currents

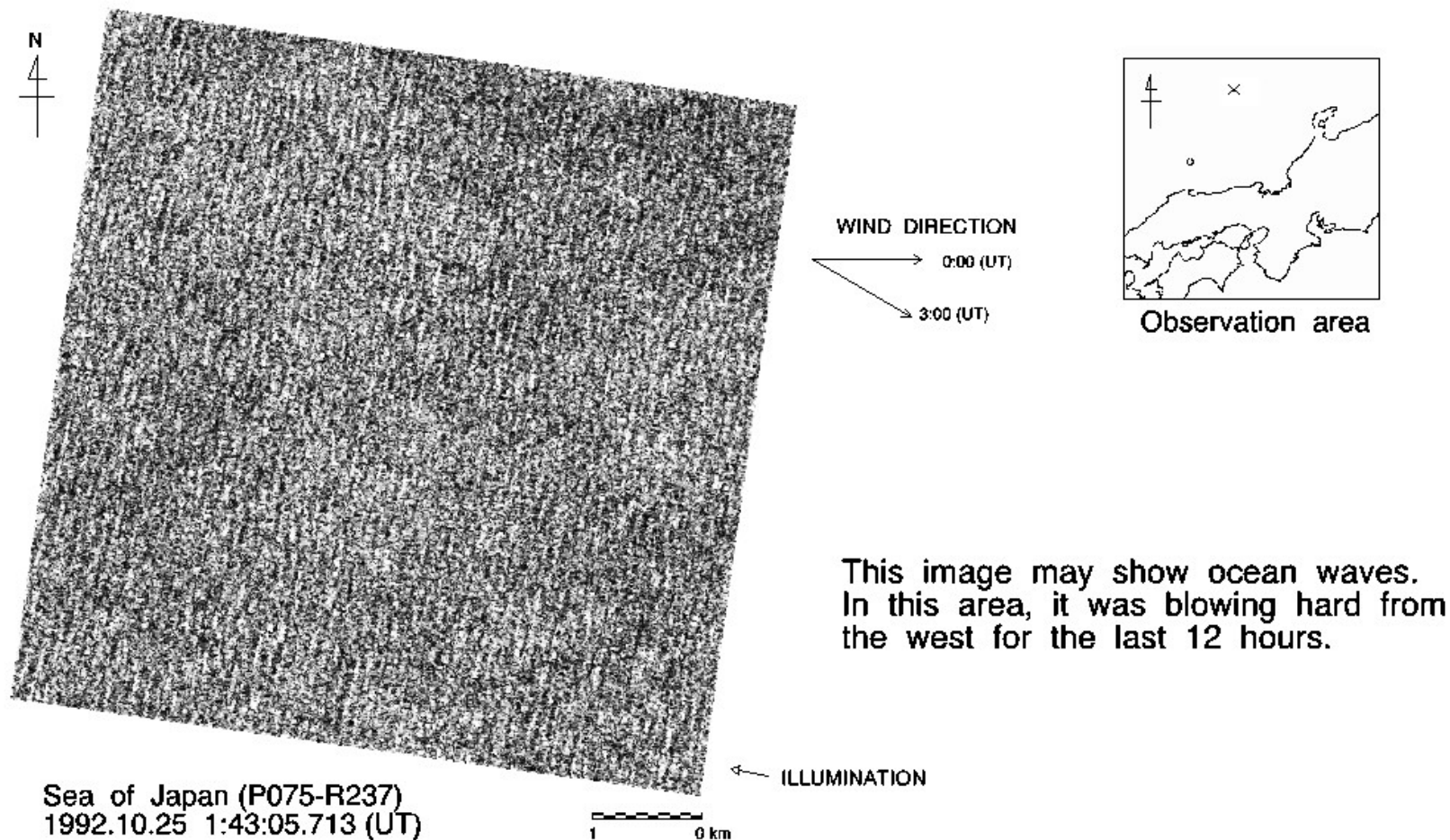
Ship Wakes

Slicks



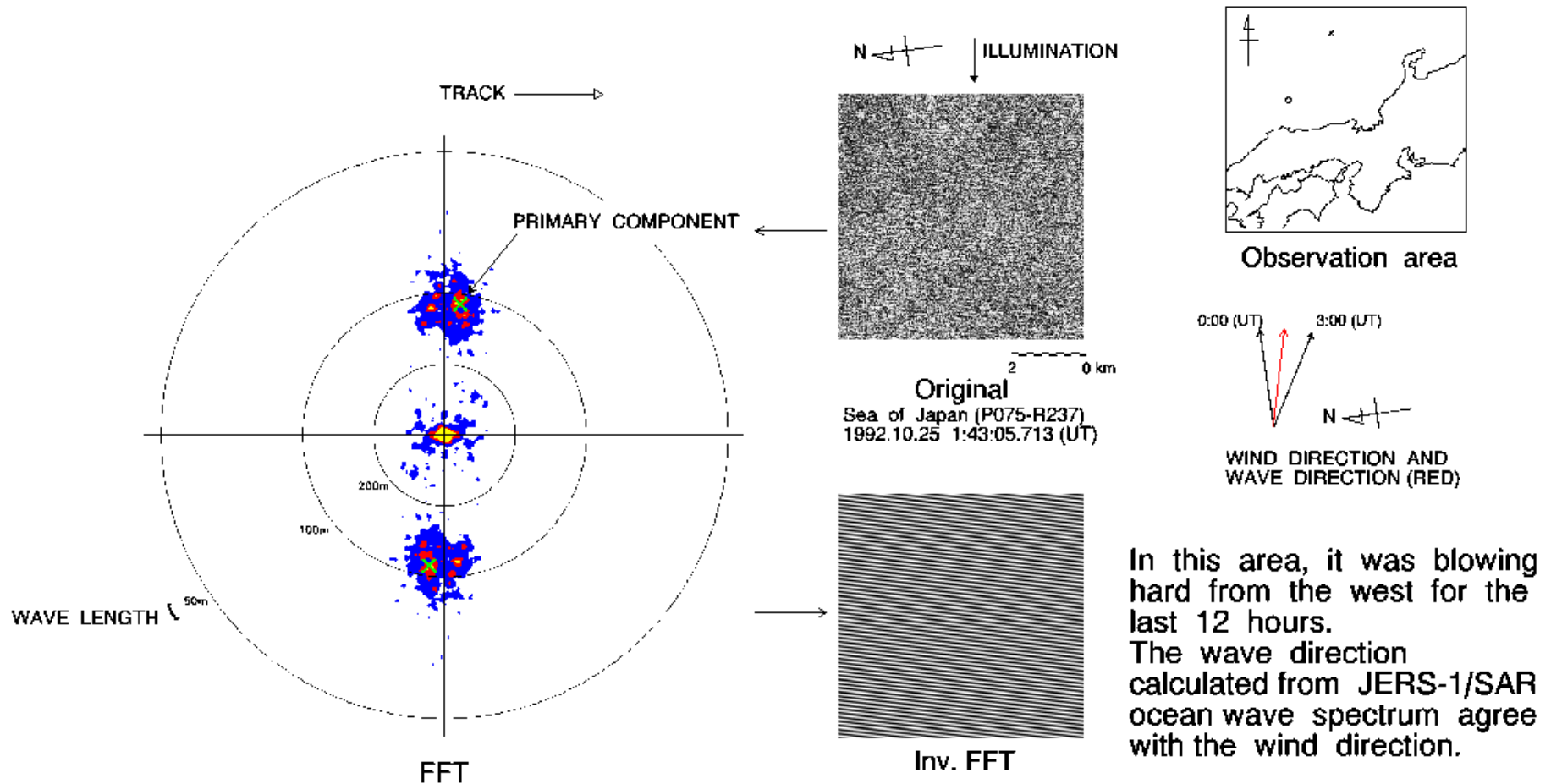
# Large Wave Characteristics

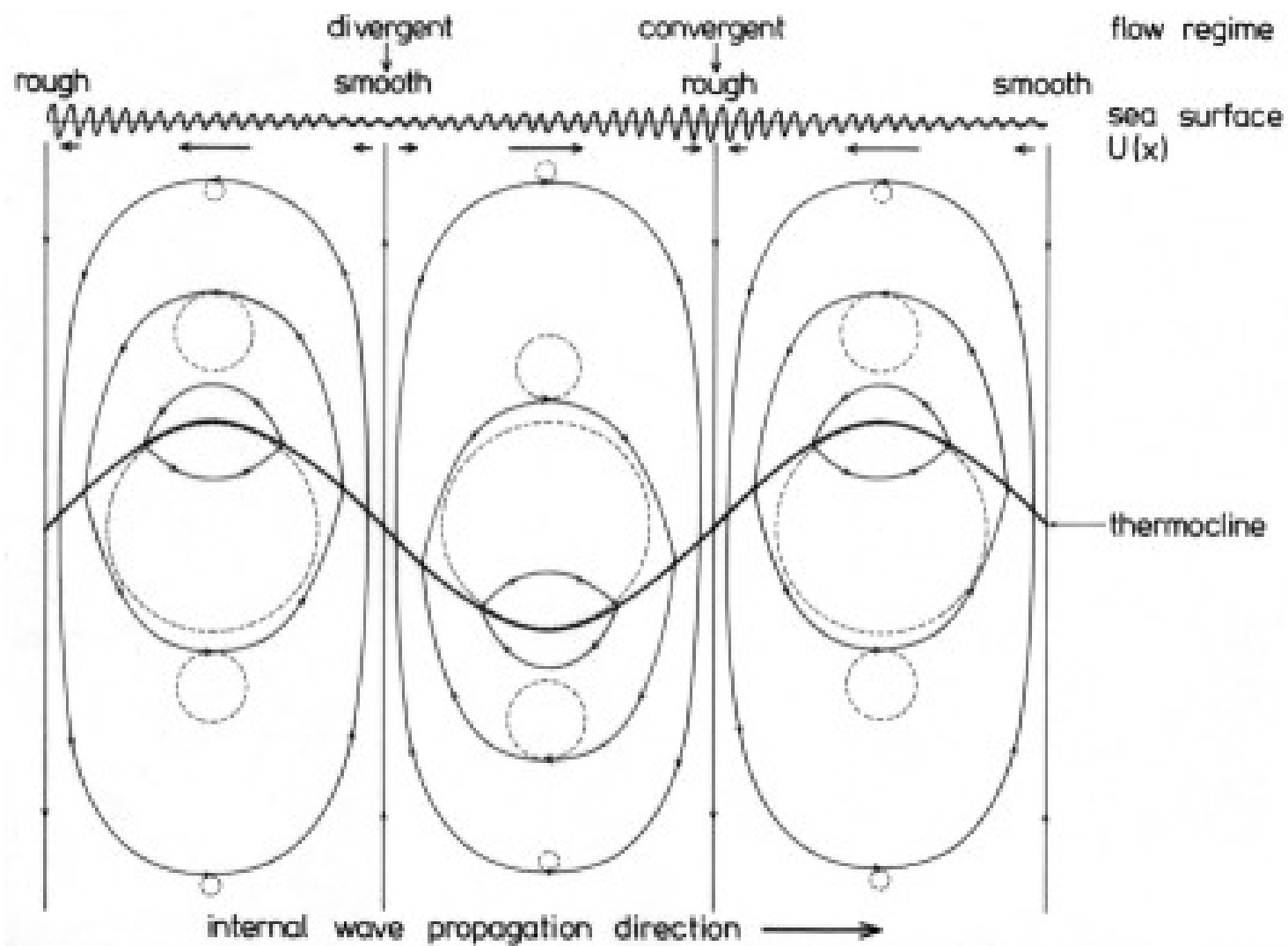
## JERS-1/SAR IMAGE OF THE SEA OF JAPAN



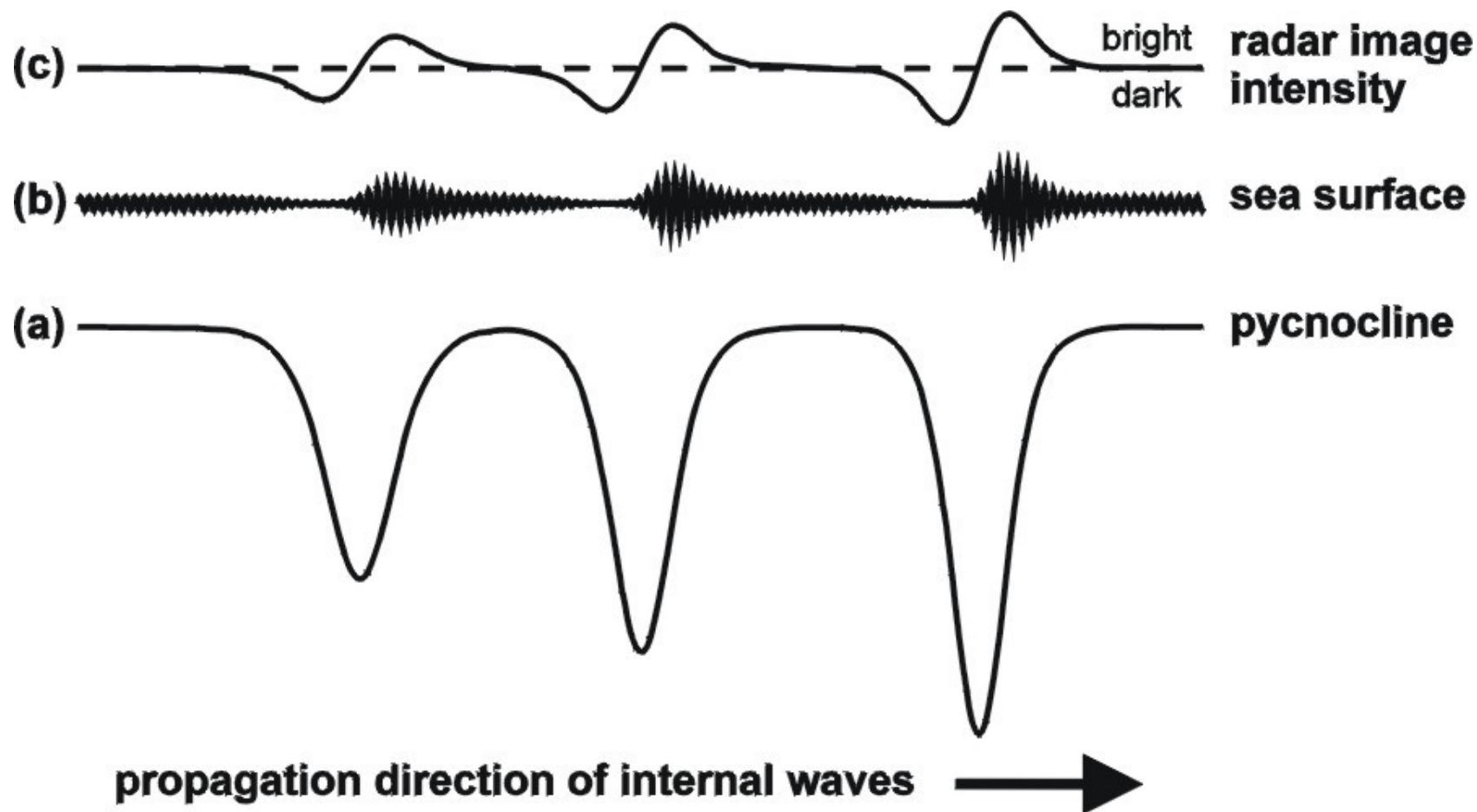
This image may show ocean waves.  
In this area, it was blowing hard from  
the west for the last 12 hours.

# JERS-1/SAR OCEAN WAVE SPECTRUM











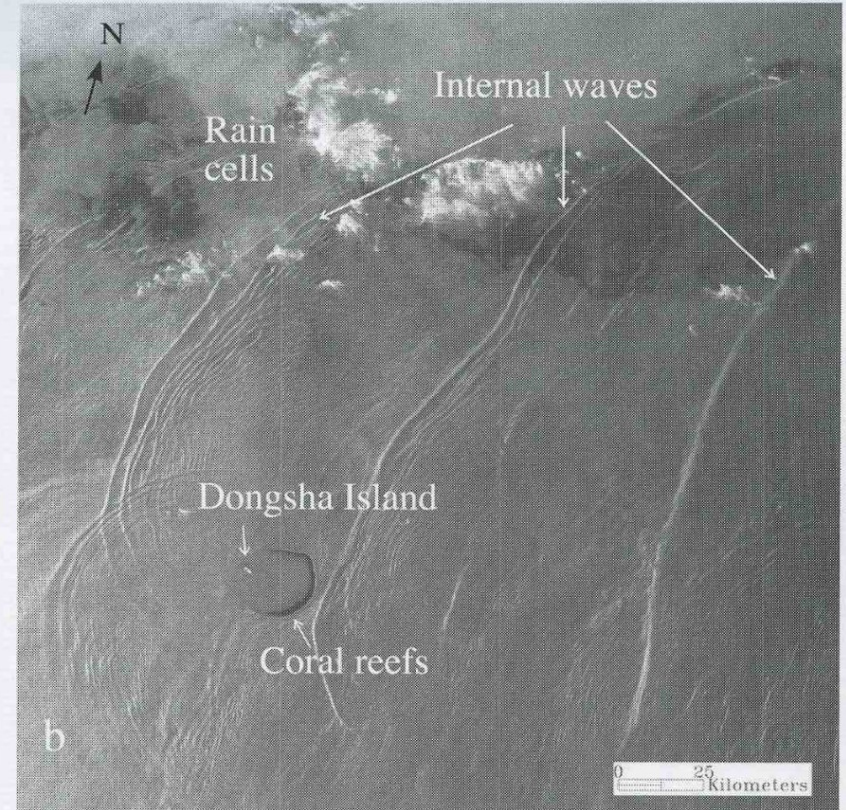
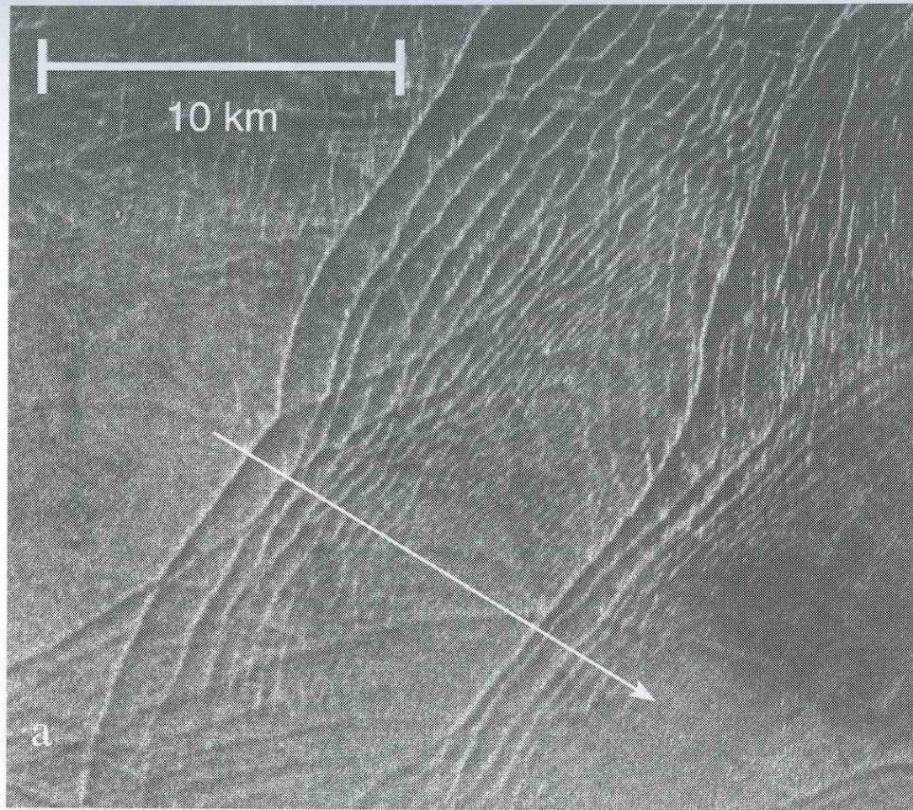


Figure 13.18. SAR observations of internal waves. (a) Propagation of internal waves on the continental slope off New Jersey taken from a Standard beam RADARSAT image taken on 2240 UTC on 31 July, 1996. The wave crests are approximately parallel to the isobaths. The white line and arrow show the direction of wave propagation (Figure 2 from Li *et al.*, 2000, reprinted from *Johns Hopkins APL Technical Digest* with permission, figure © 2000 The Johns Hopkins University Applied Physics Laboratory, RADARSAT data © Canadian Space Agency/Agence Spatiale Canadienne 1996. Processed and distributed by RADARSAT International, courtesy Pablo Clemente-Colón). (b) RADARSAT ScanSAR-Wide image taken on April 26, 1998 of the westward propagation of internal waves in the South China Sea and in the vicinity of Dongsha Island and its surrounding coral reefs. The image measures about 240 km by 240 km. Pixel size in original image is 100 m. See text for further description (Adapted from Figure 5 of Hsu and Liu, 2000, figure © 2000 Canadian Aeronautics and Space Institute, RADARSAT data © Canadian Space Agency/Agence Spatiale Canadienne 1996. Processed and distributed by RADARSAT International, courtesy Antony Liu).



# SAR applications

ICE

ice edge

ice motion

ice thicknesss

Waves

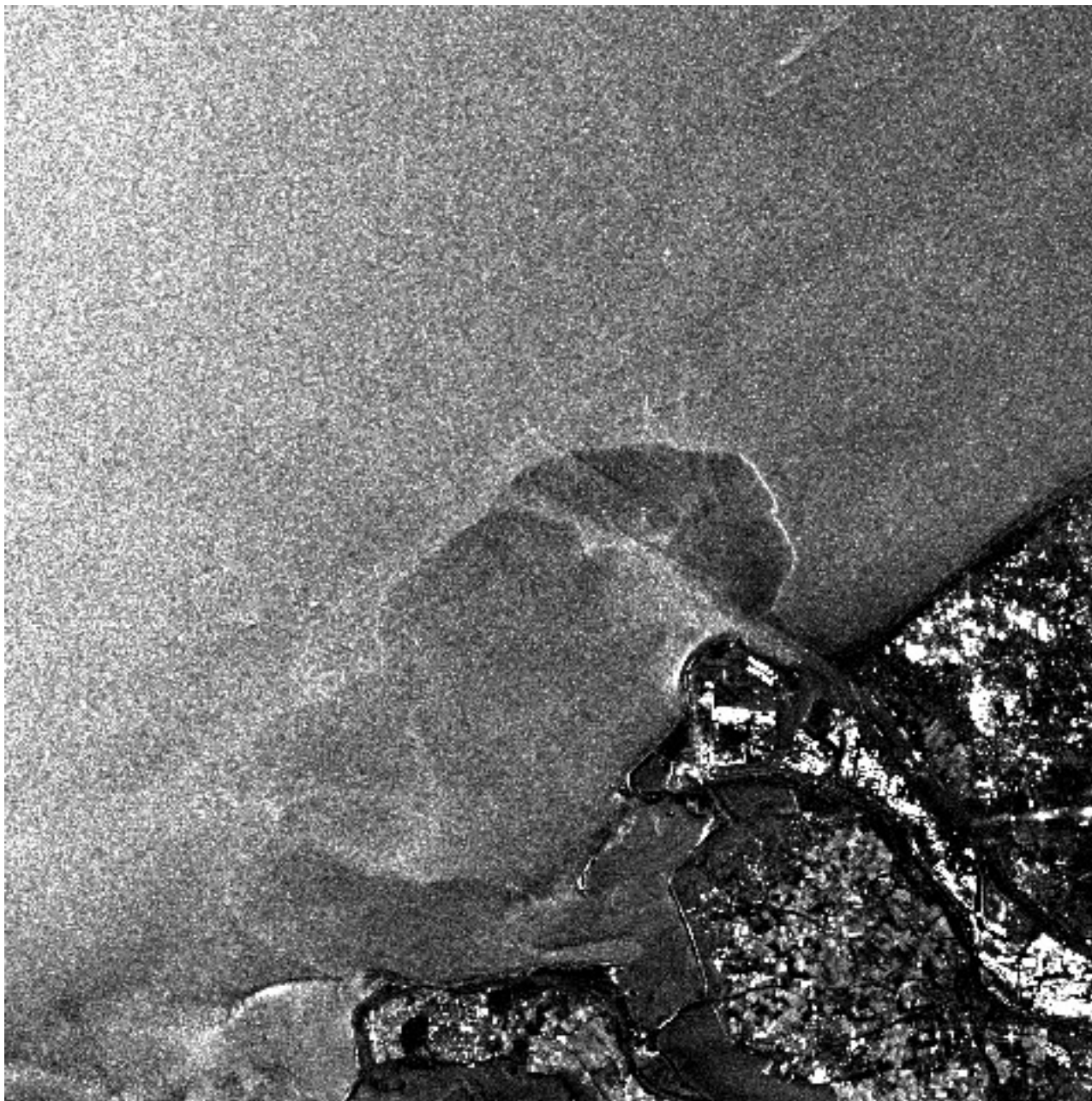
Winds

Currents

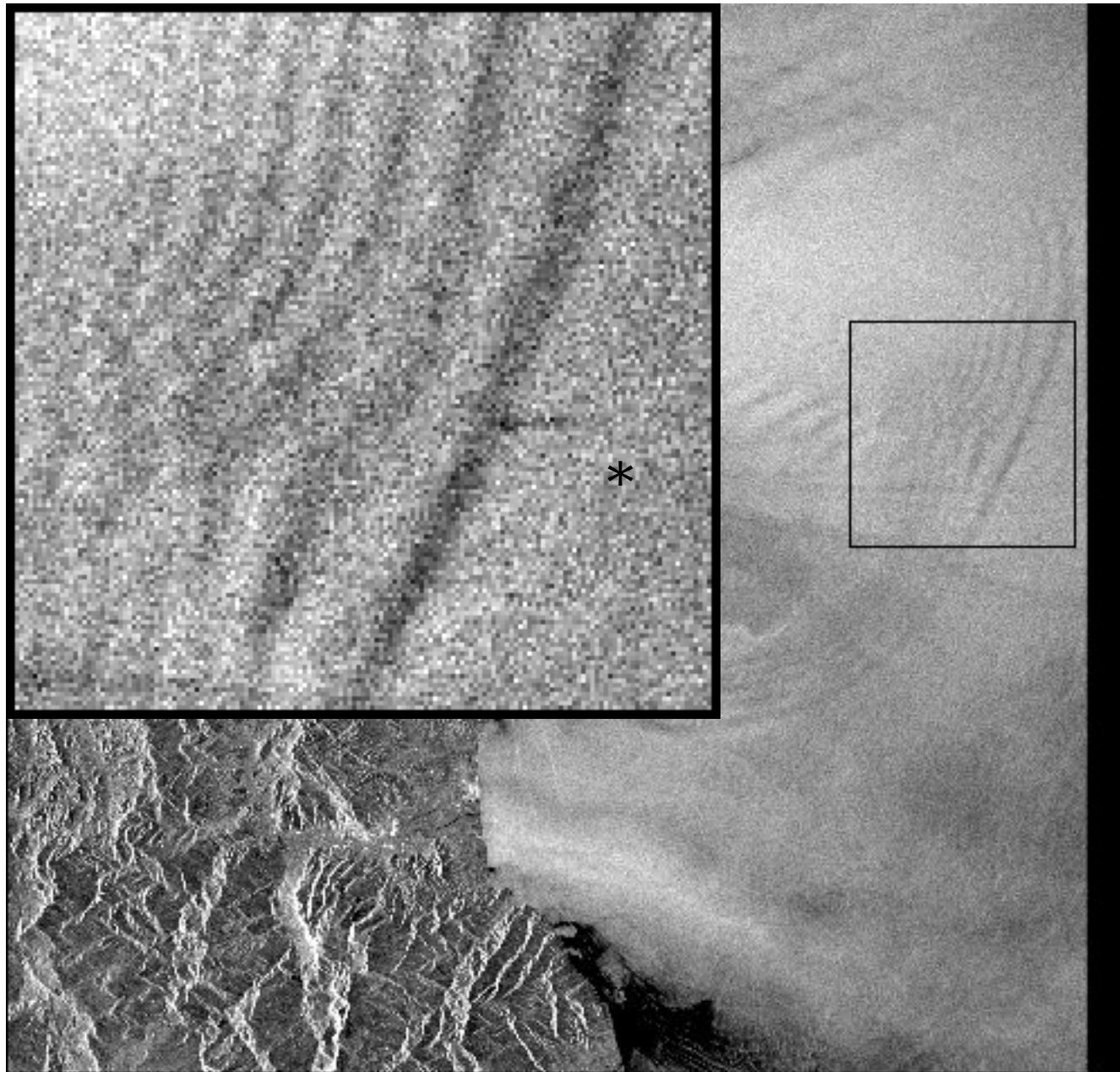


Ship Wakes

Slicks



**\*\***<http://marsais.nerisc.>



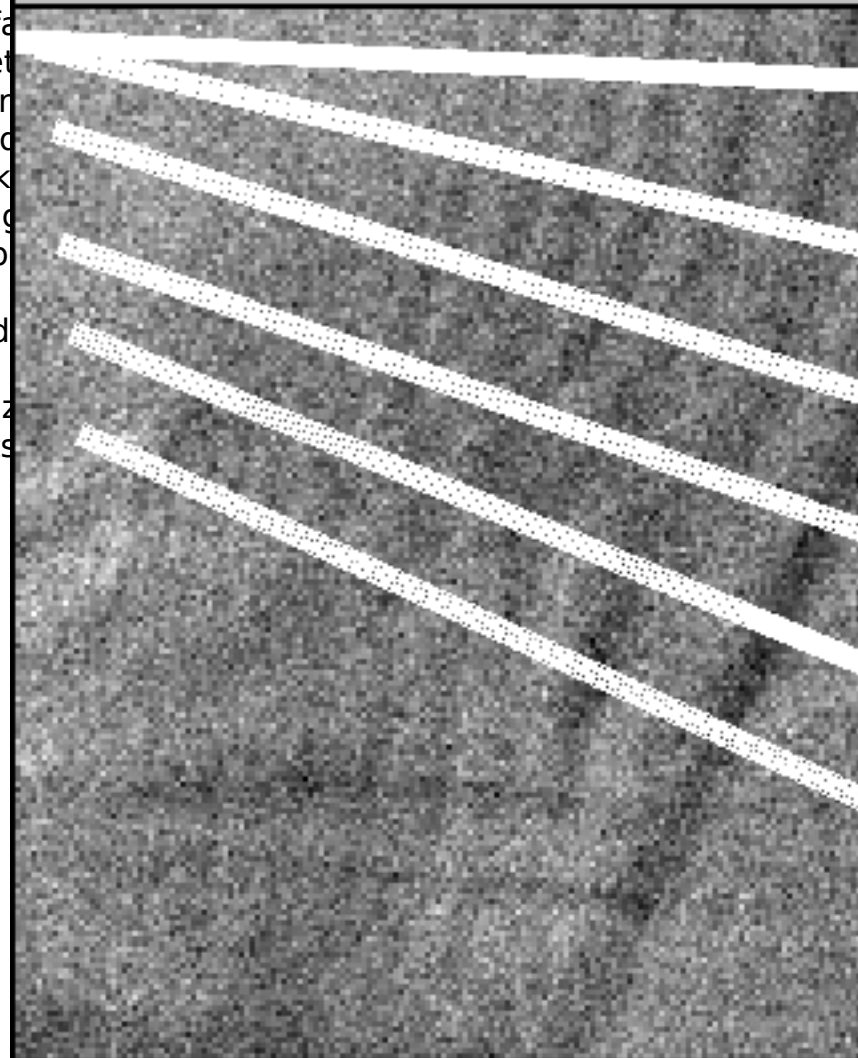
Input

- \* Calib
  - \* Seas
- profiles (
- \* Seas
- direction
- \* Unde
  - \* Surfa
- from met
- \* Inter
- identified
- \* Look
- assuming
- sheet1.p

Output d

- \* Horiz
- transects

All transects used in the shown sub  
x0=751., y0=469., frame=0711, orbit

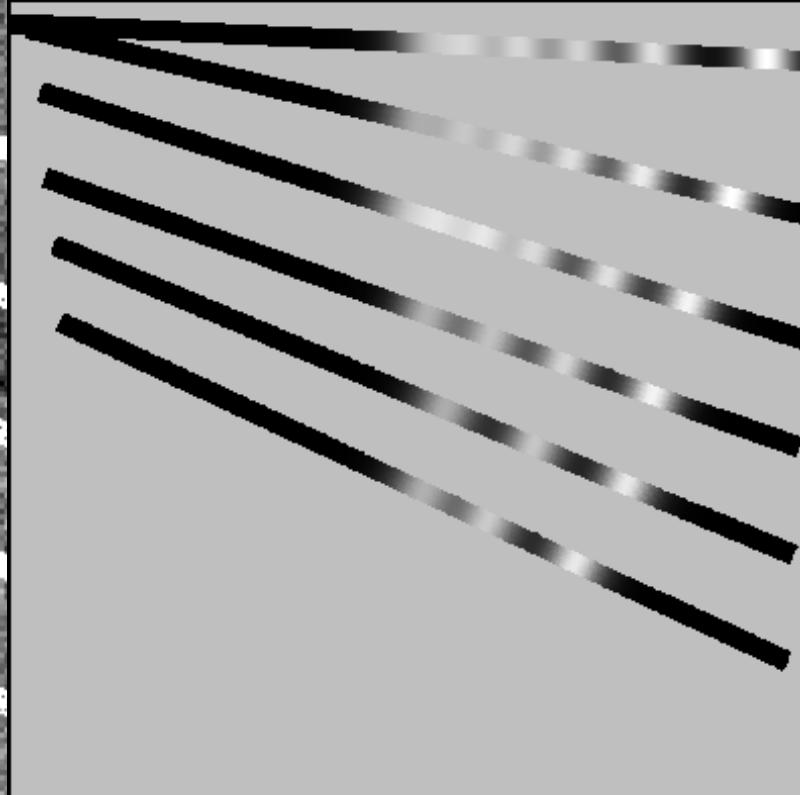


Surface current profiles of the subframe at  
x0=751., y0=469., frame=0711, orbit=10667

Densities: 1030.0kgm<sup>-3</sup>, 1031.0kgm<sup>-3</sup>

Total water depth: 1000m

Upper water layer depth: 100m



Current Speed [ms<sup>-1</sup>]

0.00 0.09 0.18 0.27 0.36



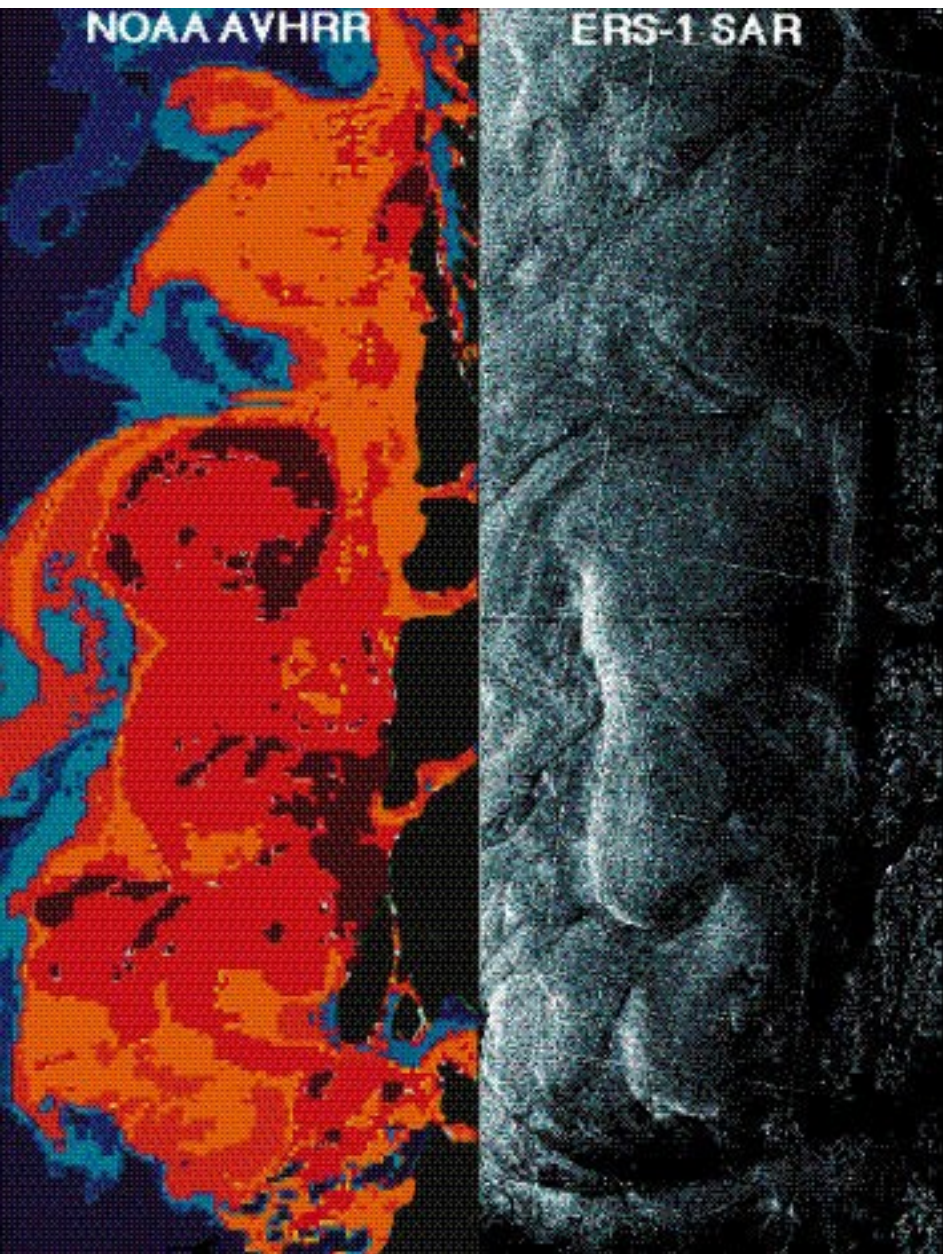


Figure 1.62 Comparison of a 1 km resolution AVHRR image acquired at 14:20 on 3/10/92 (white is 14°C and purple is 12°C; + denotes buoy position; land is masked in green and clouds in black) and a 100m resolution ERS-1 SAR ( Copyright ESA 1992 ) image acquired at 21:35 on 3/10/92. Both images cover the same 100 km x 300 km region off the west coast of Norway between 59°N and 62°N. (Acknowledgement: J.A. Johannessen et al., 1994).

# SAR applications

ICE

ice edge

ice motion

ice thicknesss

Waves

Winds

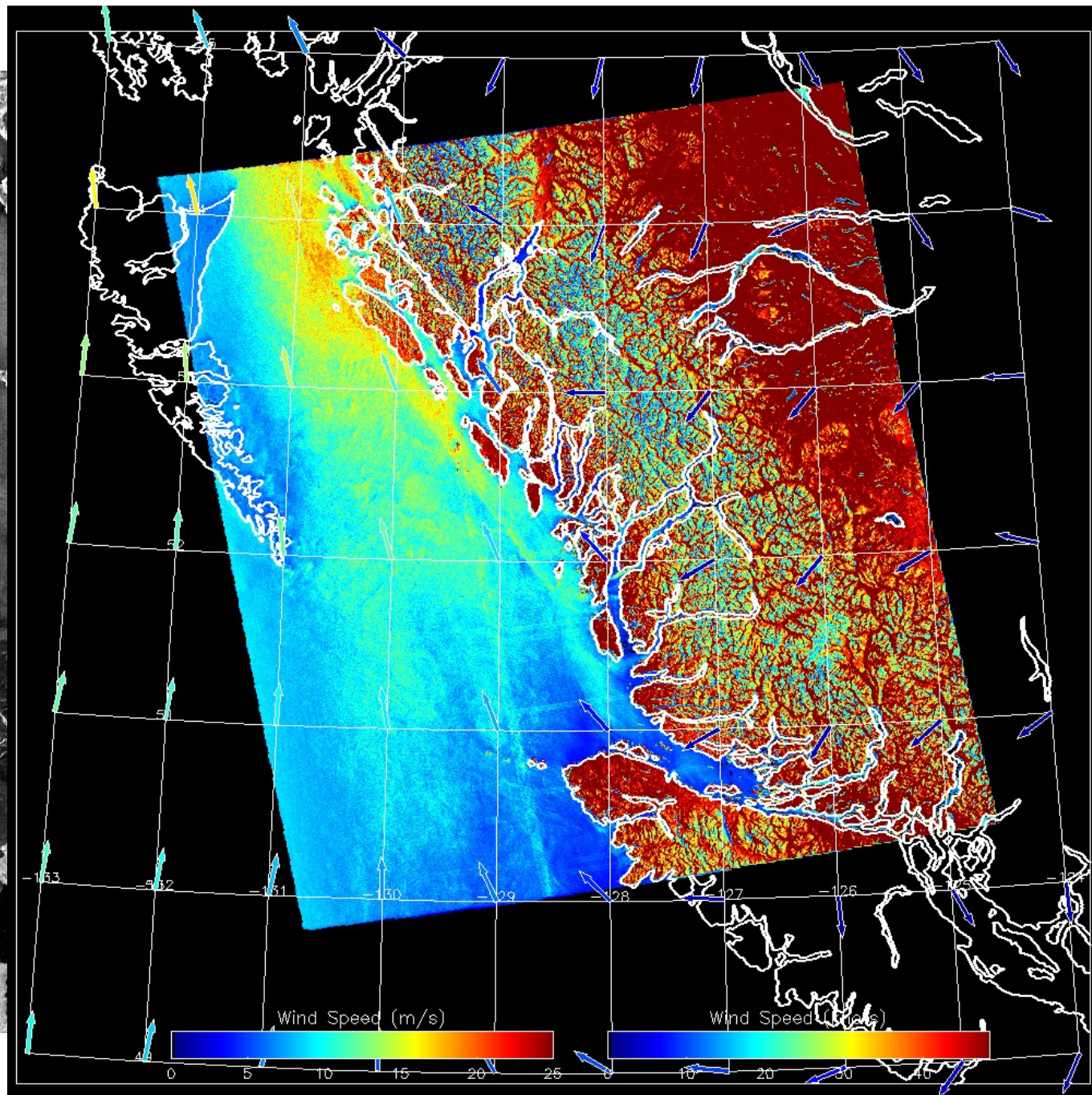


Currents

Ship Wakes

Slicks





# SAR applications

ICE

ice edge

ice motion

ice thicknesss

Waves

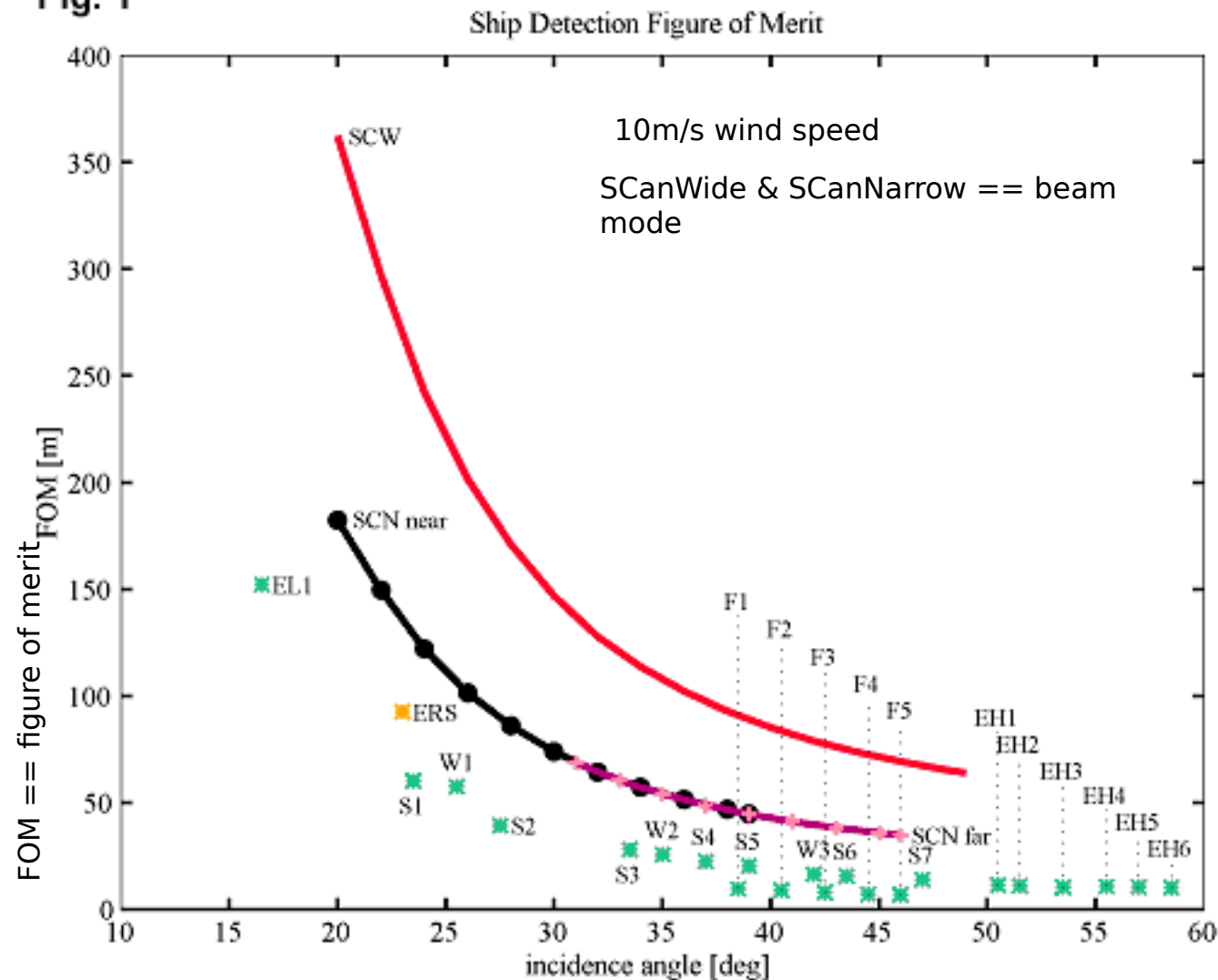
Winds

Currents

Ship Wakes



Slicks

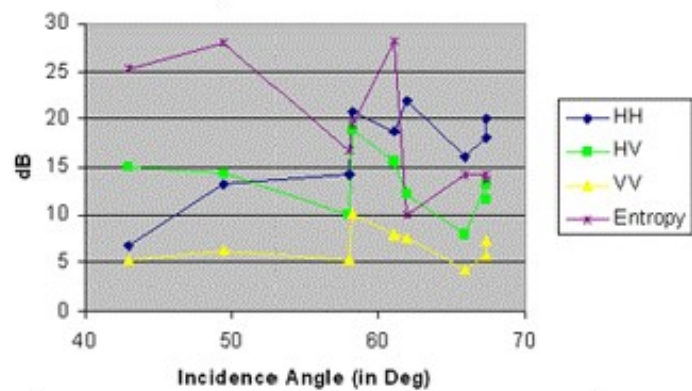
**Fig. 1**

Vachon, P.W., J.W.M. Campbell, C. Bjerkelund, F.W. Dobson, and M.T. Rey; "Validation of Ship Detection by the RADARSAT SAR"; submitted

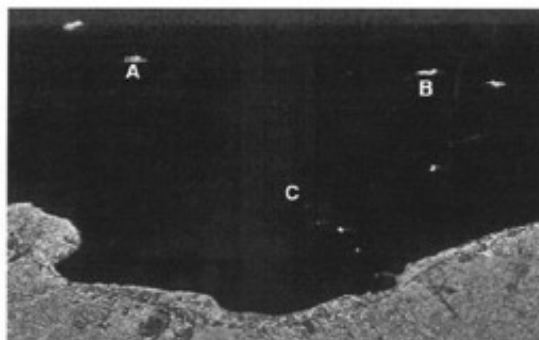
to Proc. Pacific Ocean Remote Sensing Conference (PORSEC'96), 13-16 Aug. 1996, Victoria, Canada



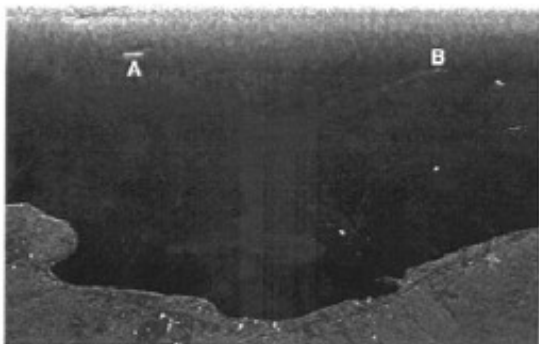
# Ship-Sea Contrast

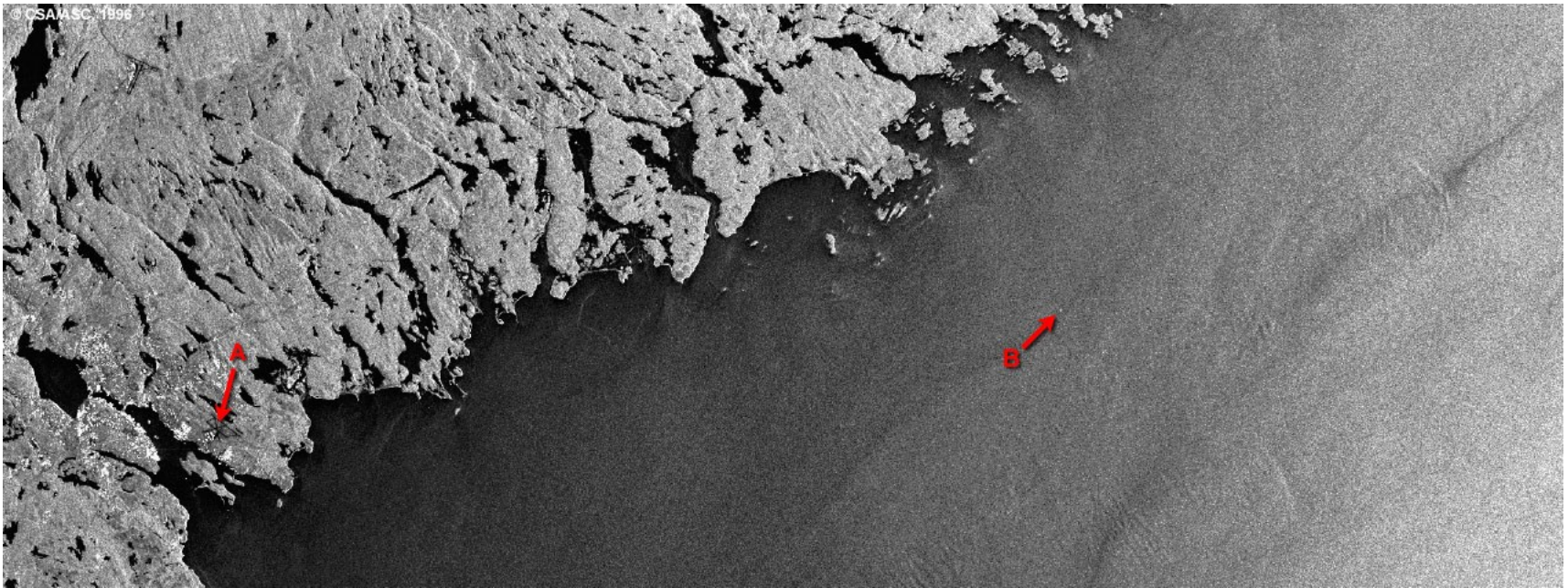


## HV Polarization



## HH Polarization

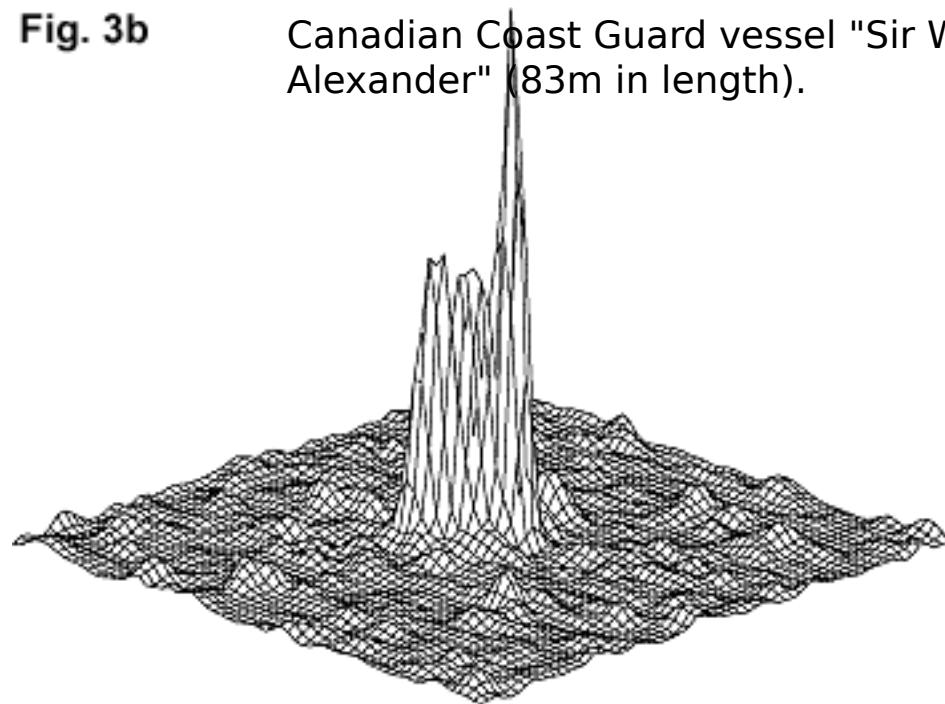




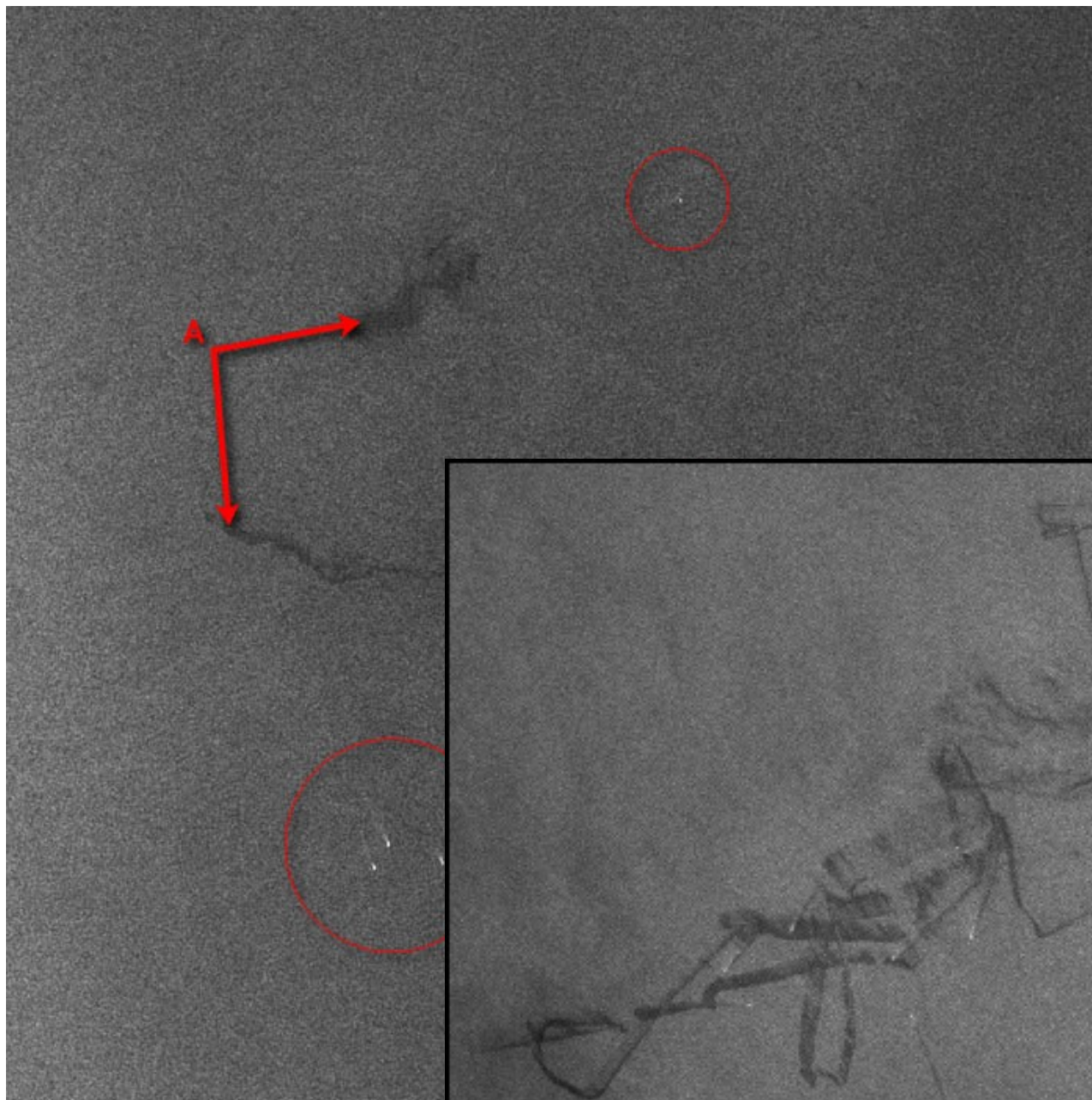
**Fig. 3b**

Canadian Coast Guard vessel "Sir William Alexander" (83m in length).

**A = airport; B = ship**







© ESA 1992

# SAR applications

ICE

ice edge

ice motion

ice thicknesss

Waves

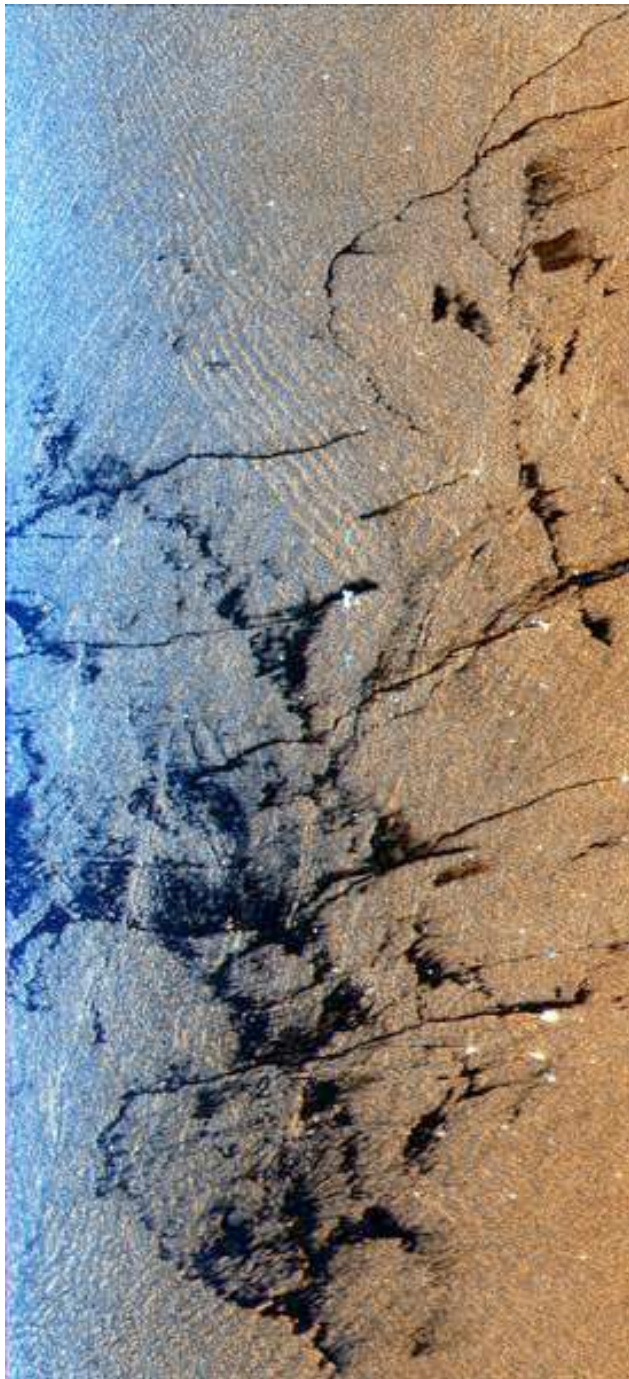
Winds

Currents

Ship Wakes

Slicks



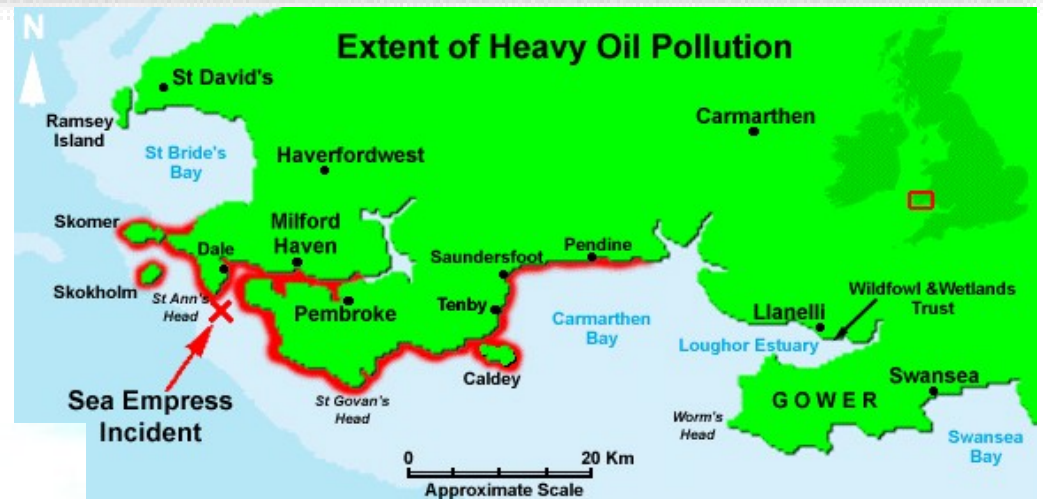
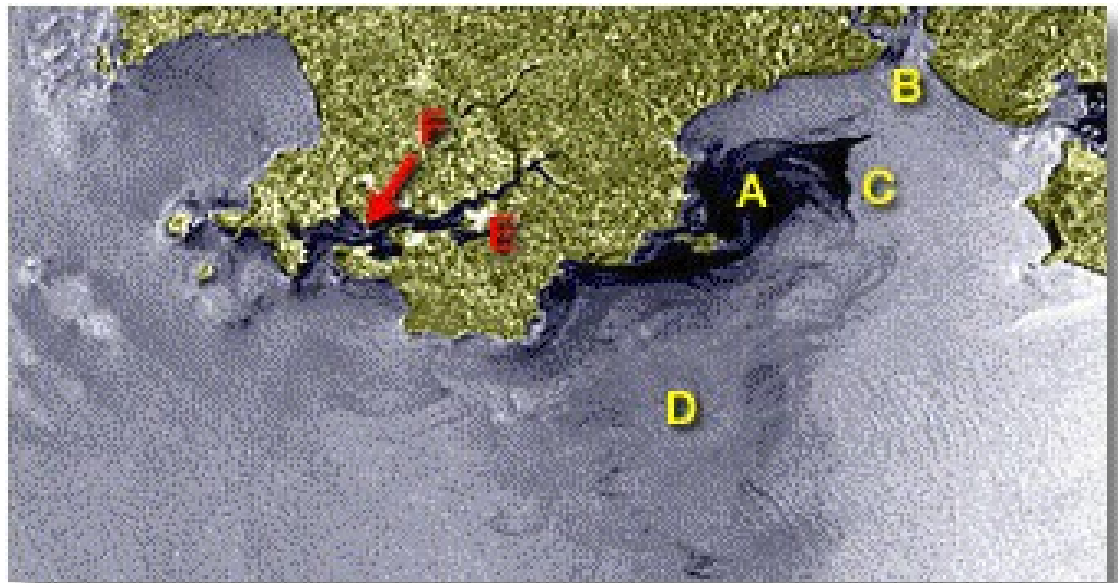


SIR-C/X-SAR (shuttle)

Offshore drilling field - Indian Ocean  
20km x 45km Oct. 9, 1994



"Sea Empress"  
Oil Spill Monitoring  
Milford Haven, Wales,  
United Kingdom  
February 22, 1996



## Interesting SAR Sites

### SAR Missions

Airbone High-resolution Multiparameter Synthetic Aperture Radar (Japan)

Heriot-Watt University, Department of Physics

SIR-C/X-SAR Space Radar Images of Earth (NASA JPL)

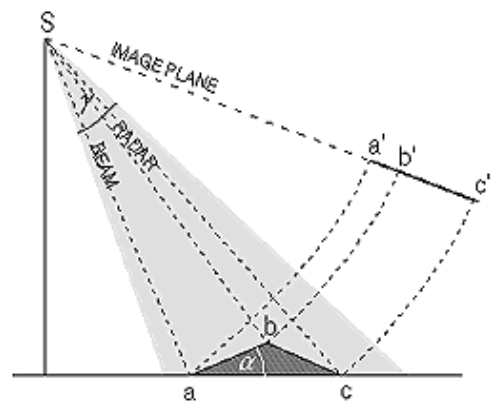
Alaska SAR Facility

# **SAR applications**

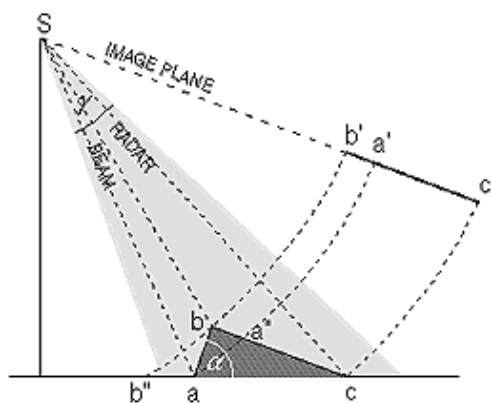
LAND



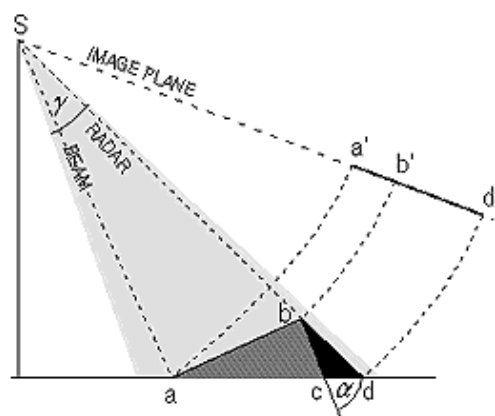
## Geometric Distortion



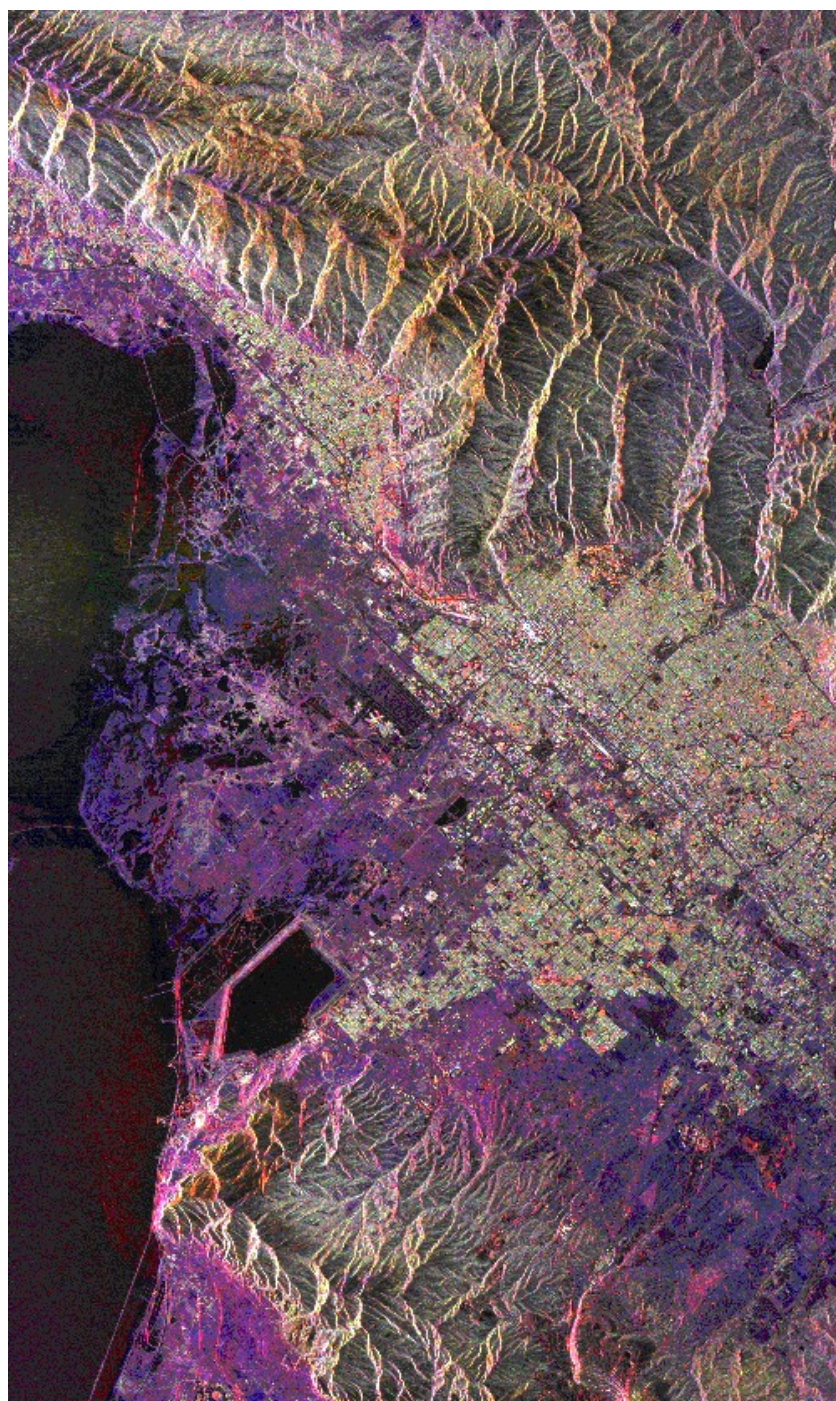
**Foreshortening**



**Layover**



**Shadowing**





## **Oxford County, Ontario**

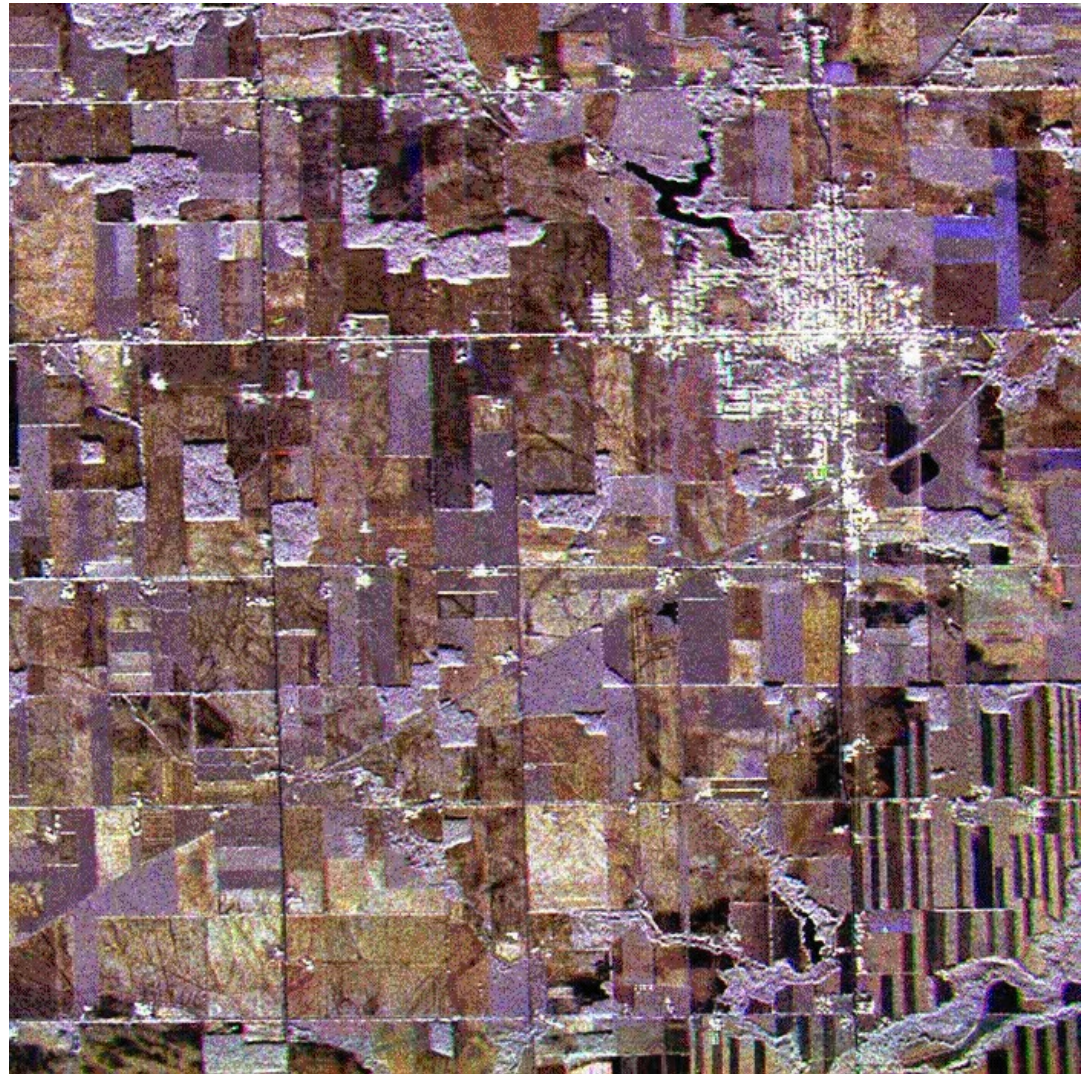
**HH Polarization:**

**R=May 22, 1990**

**G=May 23, 1990**

**B=May 25, 1990**

HH polarized microwaves penetrate vegetation to a greater degree than VV and hence respond to variations in plant volume and underlying soil moisture. This can decrease class separability at low plant density and increase at high density.





## **Oxford County, Ontario**

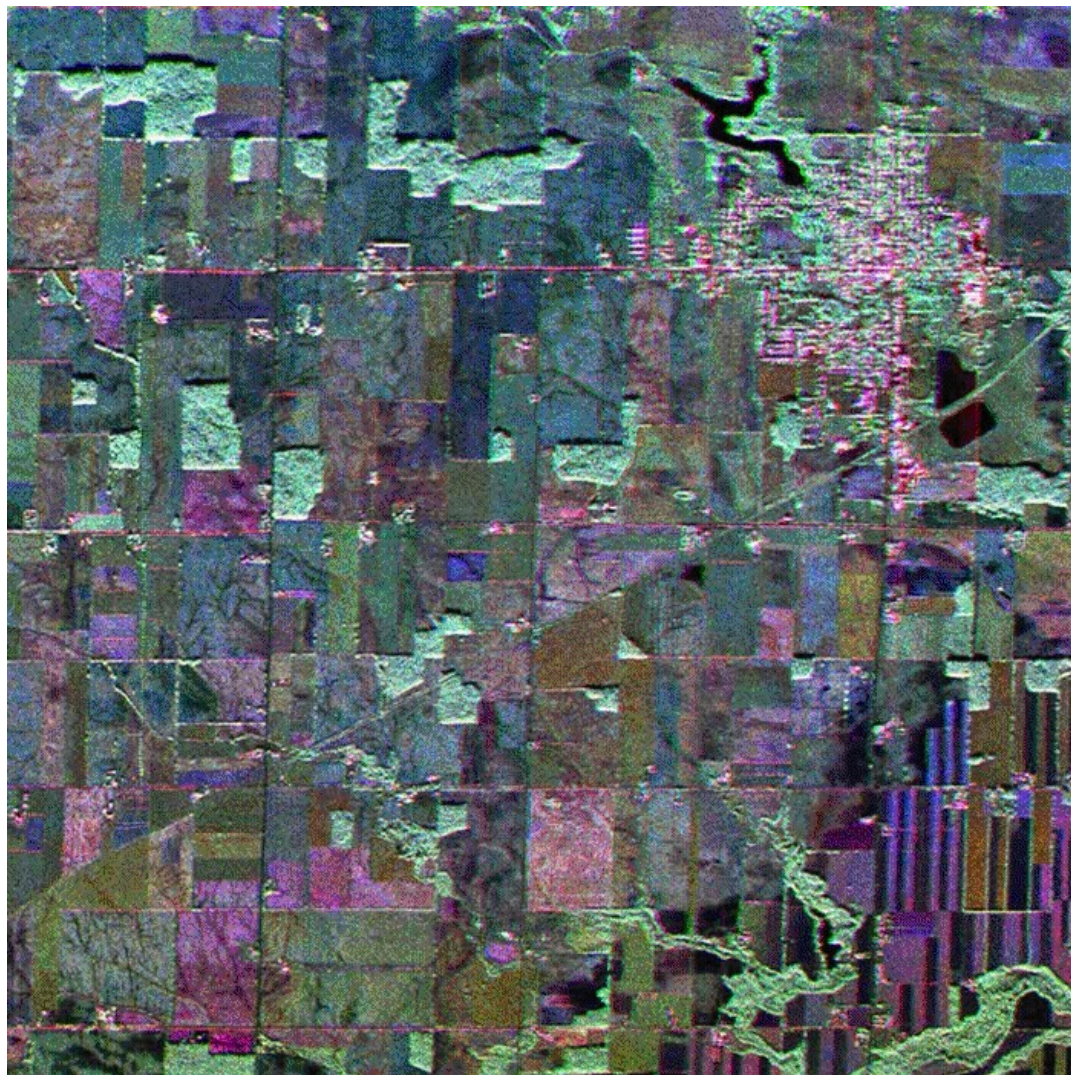
**VV Polarization:**

**R=May 22, 1990**

**G=May 23, 1990**

**B=May 25, 1990**

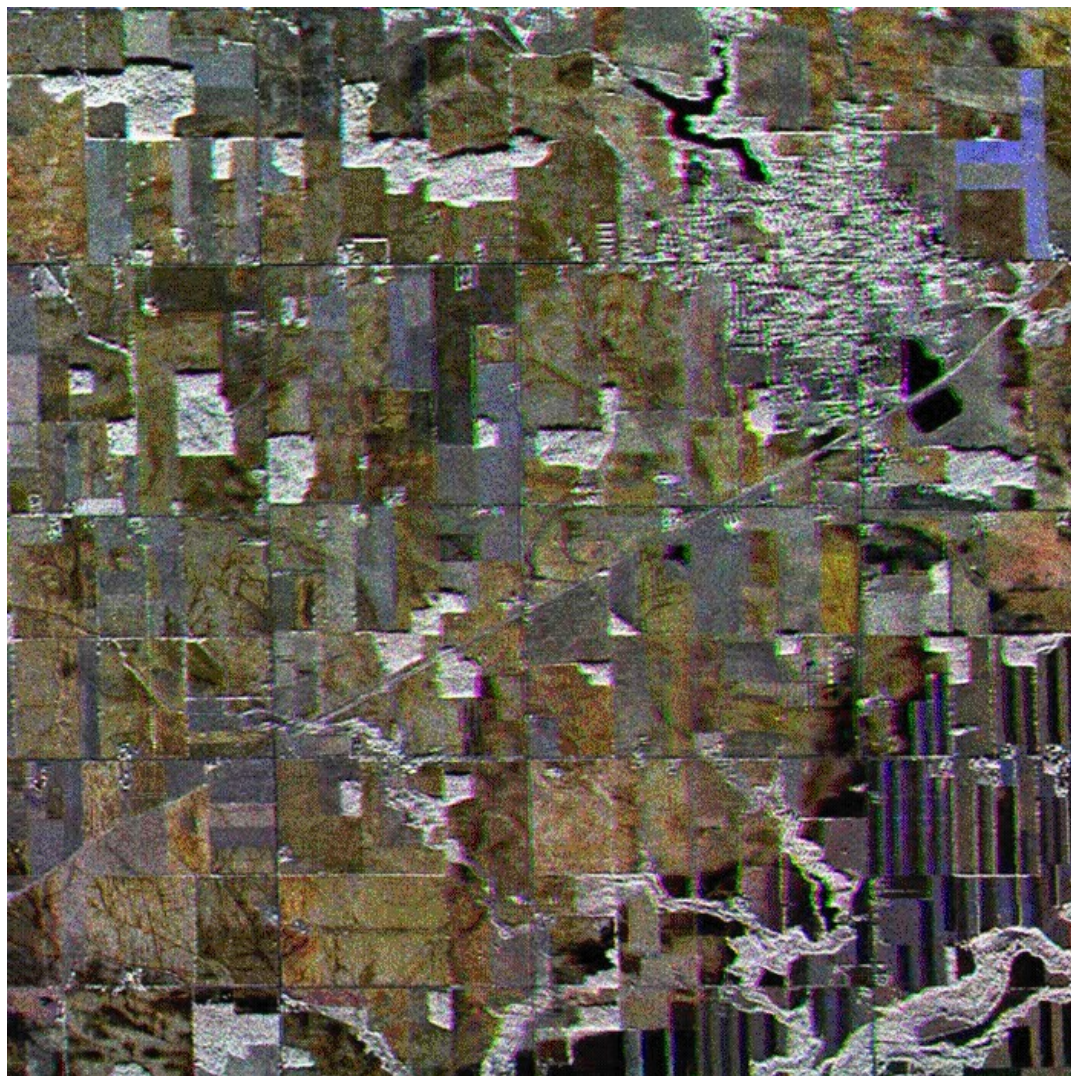
Vertically polarized microwaves couple with the vertical structure of crops, providing good contrast among different crop types. In this C-VV image, the difference in crop structure and planting dates between winter wheat and rye can be detected. The attenuation of VV microwaves by alfalfa crops separates these fields from other early season crops better than HH.





**Oxford County, Ontario,  
HV polarization:  
R=May 22, 1990  
G=May 23, 1990  
B=May 25, 1990**

Forested areas act as strong depolarizers of microwave signals and as a result, wooded areas are more easily separated from cropped and bare agricultural fields than with like polarized data.

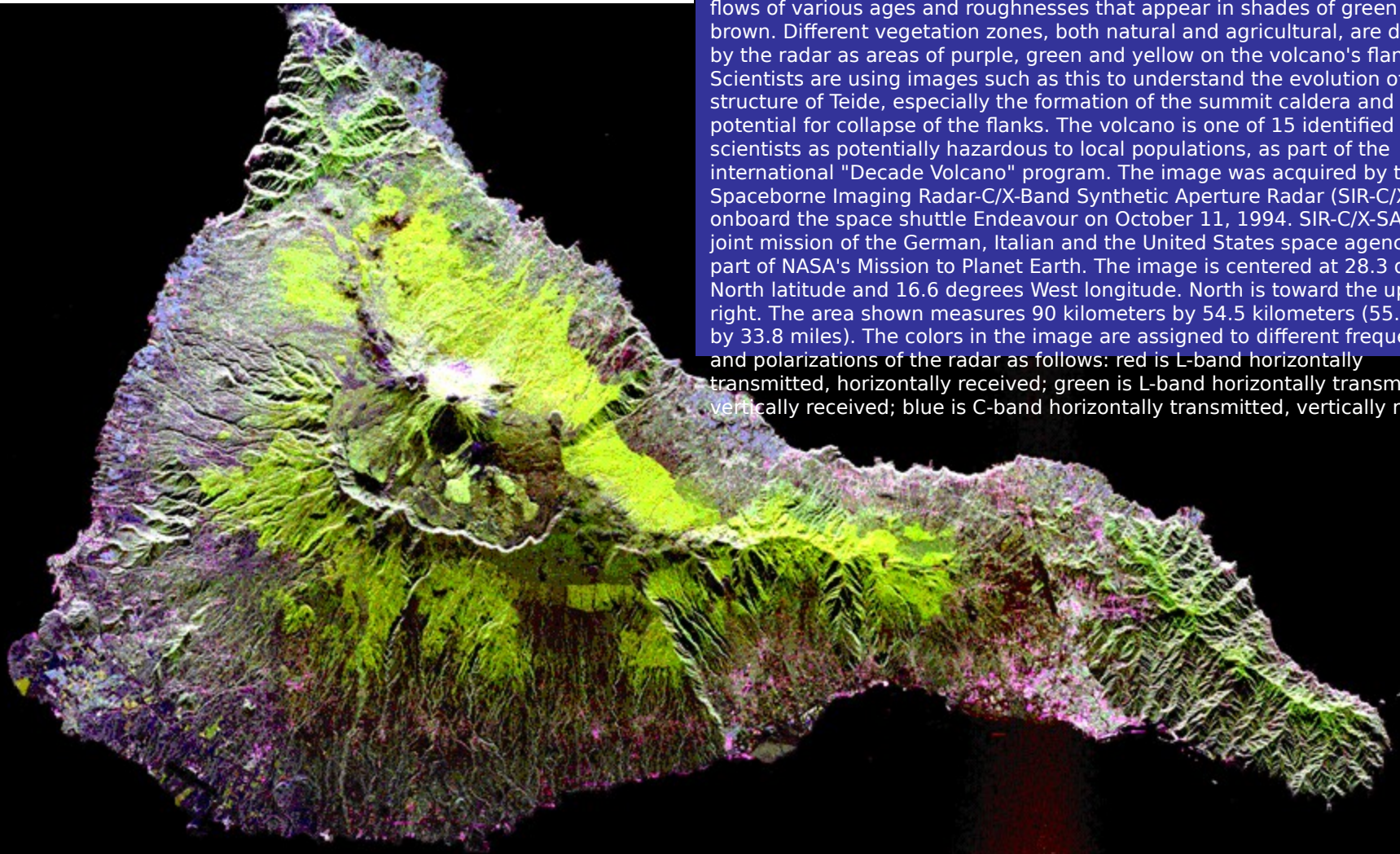




R - L-band HH  
G - L-band HV  
B - C-band HV

## Teide Volcano

This radar image shows the Teide volcano on the island of Tenerife in the Canary Islands. The Canary Islands, part of Spain, are located in the eastern Atlantic Ocean off the coast of Morocco. Teide has erupted only once in the 20th Century, in 1909, but is considered a potentially threatening volcano due to its proximity to the city of Santa Cruz de Tenerife, shown in this image as the purple and white area on the lower right edge of the island. The summit crater of Teide, clearly visible in the left center of the image, contains lava flows of various ages and roughnesses that appear in shades of green and brown. Different vegetation zones, both natural and agricultural, are detected by the radar as areas of purple, green and yellow on the volcano's flanks. Scientists are using images such as this to understand the evolution of the structure of Teide, especially the formation of the summit caldera and the potential for collapse of the flanks. The volcano is one of 15 identified by scientists as potentially hazardous to local populations, as part of the international "Decade Volcano" program. The image was acquired by the Spaceborne Imaging Radar-C/X-Band Synthetic Aperture Radar (SIR-C/X-SAR) onboard the space shuttle Endeavour on October 11, 1994. SIR-C/X-SAR, a joint mission of the German, Italian and the United States space agencies, is part of NASA's Mission to Planet Earth. The image is centered at 28.3 degrees North latitude and 16.6 degrees West longitude. North is toward the upper right. The area shown measures 90 kilometers by 54.5 kilometers (55.8 miles by 33.8 miles). The colors in the image are assigned to different frequencies and polarizations of the radar as follows: red is L-band horizontally transmitted, horizontally received; green is L-band horizontally transmitted, vertically received; blue is C-band horizontally transmitted, vertically received.



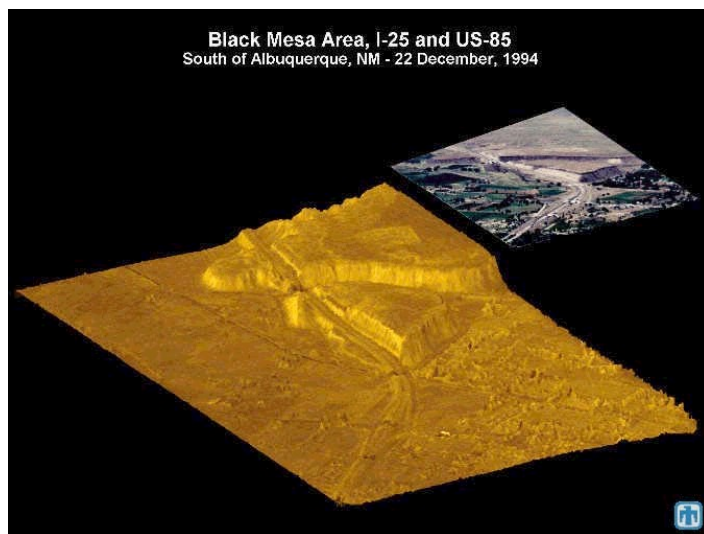
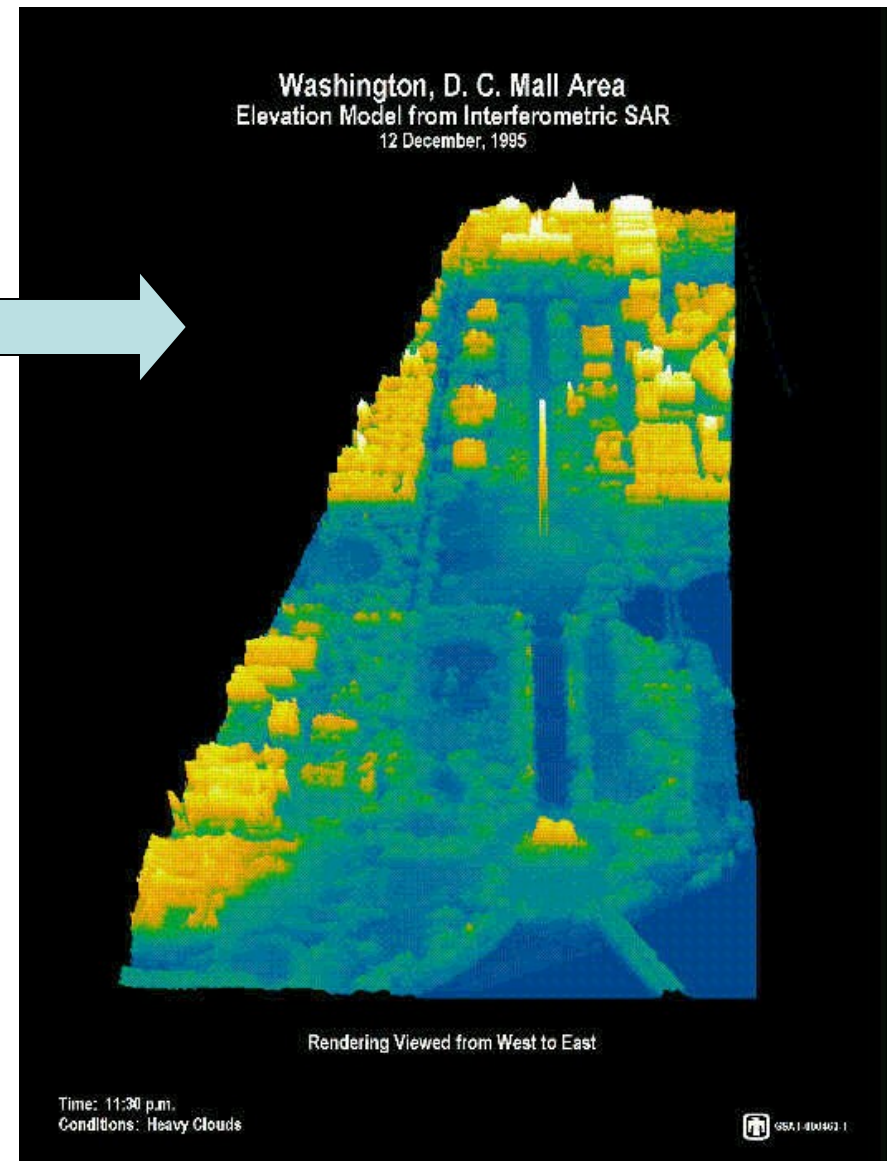
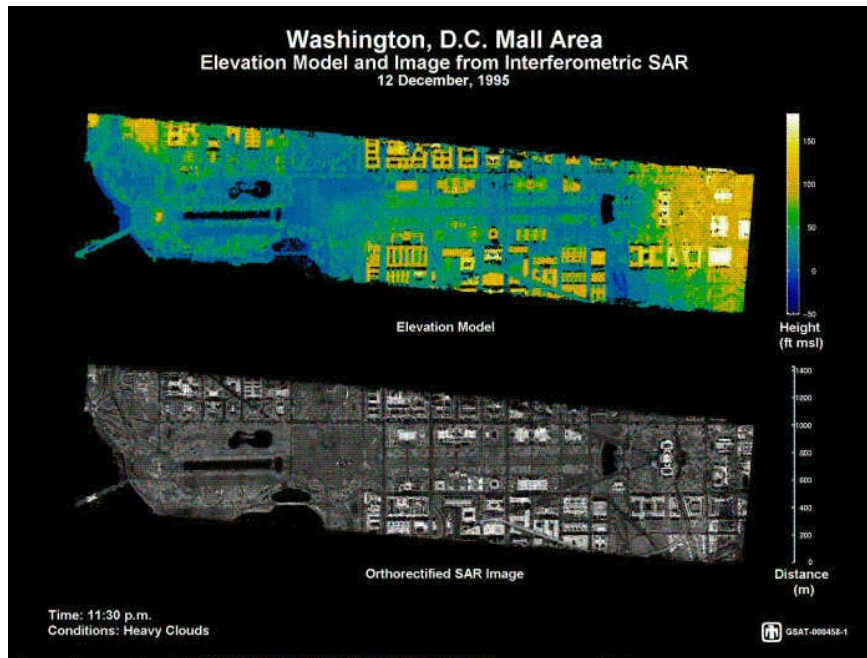




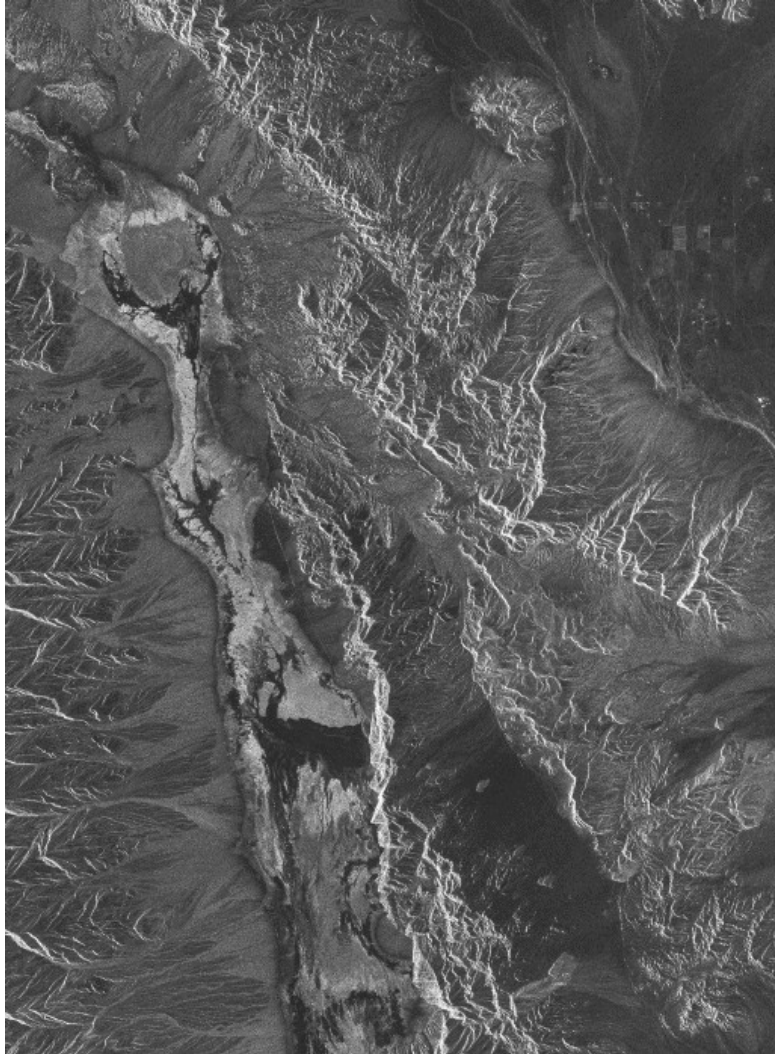
One of the properties of radar pulses gave rise to an extraordinary image acquired from SIR-A in November of 1981. The color scene below is a Landsat subimage of the Selma Sand Sheet in the Sahara Desert within northwestern Sudan. Because dry sand has a low dielectric constant, radar waves can penetrate these small particles to depths of 10 feet (several meters) or more. The inset radar strip trending NE actually images bedrock at that general depth below the loose alluvial sand and gravel which acts as though almost invisible. A channeled subsurface topography is revealed, with valleys correlative to specularly reflecting surfaces and uplands shown as brighter.

Here is a movie showing a Landsat image fading into a SIR-C/X-SAR image of the Safsaf Oasis, Egypt

Interferometric SAR (ISAR or IFSAR) essentially produces a stereo SAR view of a scene. This allows extraction of height information.



# Seasat SAR



Death Valley



Tokyo Bay Area  
(Rainbow Bridge, Tokyo  
Bigsite, etc.) (X-band,  
VV, 5 km x 4 km; flight  
direction: right to left,  
illumination: top to  
bottom)





Downtown Area of Tokyo  
(Around Shinjyuku)  
(X-band, VV, 5 km x 4 km,  
flight direction: right to left,  
illumination: top to bottom)





Kansai International Airport (Osaka)

(X-band, VV, 5 km x 4 km,

flight direction: right to left, illumination: top to bottom)

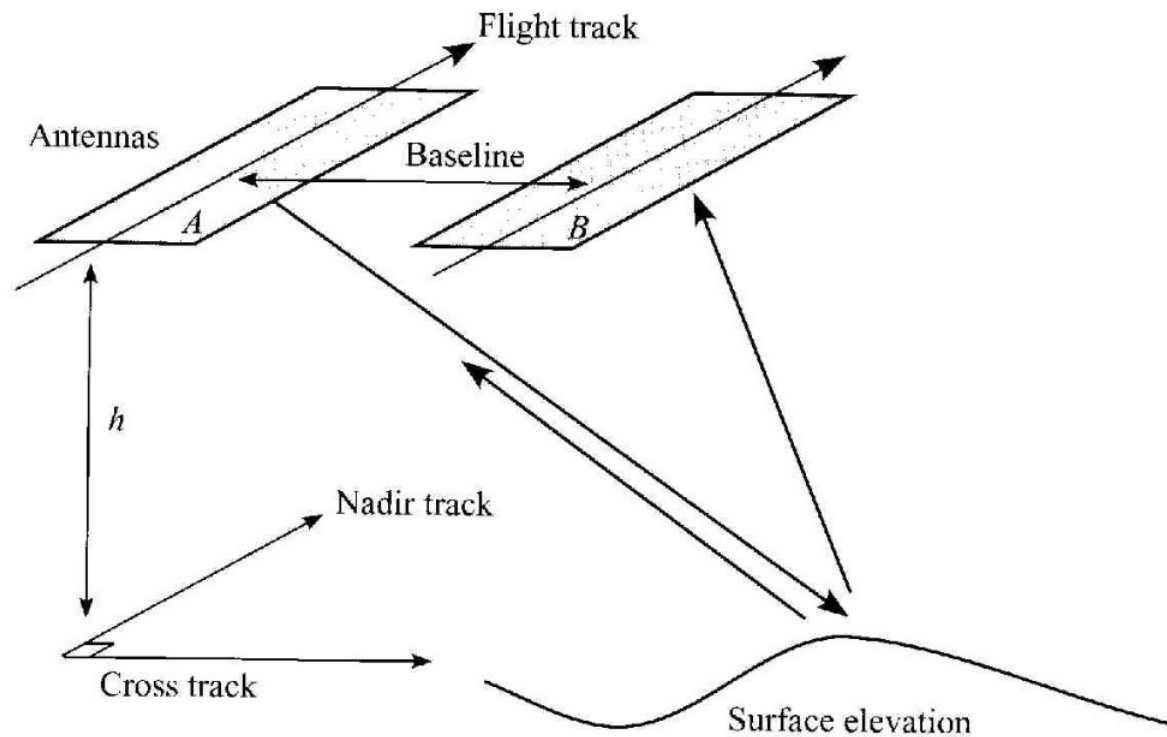


Figure 13.3. The geometry of a cross-track interferometer. The two antennas are at a specific altitude in a parallel track, and are separated by a precisely determined baseline. The antennas make simultaneous observations of the same surface area from two different locations.